



# Carbon-Based Materials as Catalyst Supports for Fischer–Tropsch Synthesis: A Review

María José Valero-Romero\*, Miguel Ángel Rodríguez-Cano, José Palomo, José Rodríguez-Mirasol\* and Tomás Cordero

Departamento de Ingeniería Química, Facultad de Ciencias, Universidad de Málaga, Andalucía Tech, Málaga, Spain

The use of carbon-based materials as catalyst supports for Fischer–Tropsch synthesis (FTS) is thoroughly reviewed. The main factors to consider when using a carbonaceous catalyst support for FTS are first discussed. Then, the most relevant and recent literature on the topic from the last 2 decades is reviewed, classifying the different examples according to the carbon structure and shape. Some aspects such as the carbon textural properties, carbon support modification (functionalization and doping), catalyst preparation methods, metal particle size and location, catalyst stability and reducibility, the use of promoters, and the catalyst performance for FTS are summarized and discussed. Finally, the main conclusions, advantages, limitations, and perspectives of using carbon catalyst supports for FTS are outlined.

**Keywords:** Fischer-Tropsch synthesis, synthesis gas (syngas), catalysts, carbon supports, catalytic performance

## OPEN ACCESS

### Edited by:

David Salinas Torres,  
University of Alicante, Spain

### Reviewed by:

Dong Hyun Chun,  
Korea Institute of Energy Research,  
South Korea  
Vladimir Mordkovich,  
Technological Institute for Superhard  
and Novel Carbon Materials, Russia

### \*Correspondence:

María José Valero-Romero  
mjvalero@uma.es  
José Rodríguez-Mirasol  
mirasol@uma.es

### Specialty section:

This article was submitted to  
Carbon-Based Materials,  
a section of the journal  
Frontiers in Materials

**Received:** 14 October 2020

**Accepted:** 30 November 2020

**Published:** 04 February 2021

### Citation:

Valero-Romero MJ,  
Rodríguez-Cano MÁ, Palomo J,  
Rodríguez-Mirasol J and Cordero T  
(2021) Carbon-Based Materials as  
Catalyst Supports for Fischer–Tropsch  
Synthesis: A Review.  
Front. Mater. 7:617432.  
doi: 10.3389/fmats.2020.617432

## INTRODUCTION

Hydrocarbons are the most widely used chemicals and fuels and are the main driving force of occidental social well-being. The major part of hydrocarbons on earth are produced from crude oil, which provide approximately 33% of the current world's primary energy requirements, followed by coal (27%) and natural gas (24%). In the past 10 years, oil consumption has grown globally by an average of 1.1% (1.1 million barrels per day), Asia being the region that has shown the highest growth, where coal consumption is still dominant. Furthermore, the global proved oil reserves account only for around 45 years at the current consumption ratio, whereas the estimates of the extent of available reserves of natural gas and coal seem to be around 50 and 132 years, respectively (BP Statistical Review, 2020). Therefore, the growing global demand for crude oil, together with its fast depletion rate, and the implementation of a more stringent environmental legislation on liquid fuels boost the use of alternative and sustainable hydrocarbon sources.

In this sense, Fischer–Tropsch synthesis (FTS) is an alternative industrial process for the production of clean liquid fuels and value-added chemicals from synthesis gas (a mixture of CO and H<sub>2</sub>), which can be derived from nonpetroleum feedstocks including natural gas, coal, and renewable biomass (mainly, lignocellulosic biomass) (Noureddin et al., 2014; Ren et al., 2019). Depending on the feedstock, the process is referred to as GTL (gas-to-liquid), CTL (coal-to-liquid), or BTL (biomass-to-liquid). Nowadays, there are large commercial FTS plants operating worldwide that produce liquid fuels and hydrocarbons from syngas obtained by partial oxidation and steam reforming of natural gas and by coal gasification (Lappas and Heracleous, 2016). However, the vast majority of BTL schemes, which uses syngas from gasification of biomass, are in the pilot or demonstration phase. The development of a commercial BTL process seems to be hindered due to the limited commercial experience in biomass gasification and its integration with fuel production

processes and to the high capital costs associated to the BTL technology (Lappas and Heracleous, 2016).

Transition metals are used in FTS process due to their considerable activity. Among them, Fe and Co are the only industrially relevant catalysts that are currently commercially used in FTS. The choice of catalyst depends primarily on the FTS operating mode: (1) the so-called low-temperature Fischer-Tropsch synthesis (LT-FTS) and (2) high-temperature Fischer-Tropsch synthesis (HT-FTS) (Steynberg, 2004). In the former case, at LT-FTS conditions (200–240°C), mostly long-chain paraffins (wax) are produced over either Fe- or Co-based catalysts. This wax is afterward (hydro) cracked in the desired product spectrum (Luque et al., 2012). On the other hand, the use of Fe-based catalysts at HT-FTS conditions (300–350°C) is typically aimed to produce short-chain unsaturated hydrocarbons, olefins (Fischer-Tropsch to olefins, FTOs), and oxygenates (Torres Galvis et al., 2012b). Furthermore, high selectivities toward gasoline-range hydrocarbons can be produced using Fe at HT-FTS conditions (Steynberg et al., 1999).

Moreover, the choice of metal also depends on the feedstock used for the FTS. When high-purity syngas is used, Co-based catalysts are preferred because of their higher intrinsic activity for FTS and higher selectivity toward linear products than those of Fe (at similar conditions). Moreover, Co-based catalysts present a low activity toward water-gas shift (WGS) and a high hydrogenation activity, therefore produce less unsaturated hydrocarbons and oxygenates, while having a higher catalyst stability (Munirathinam et al., 2018). Therefore, cobalt-based catalyst is the choice when using syngas with a  $H_2/CO \geq 2$ , as that produced from natural gas as feedstock (Aasberg-Petersen et al., 2004). On the other hand, iron-based catalysts are cheaper and widely available compared with Co-based catalysts and present a high flexibility in terms of operating conditions and poisoning, being their use possible at different temperatures and  $H_2/CO$  molar ratios (Abelló, S., and Montané, D. (2011). Exploring Iron-based Multifunctional Catalysts for Fischer-Tropsch Synthesis: A Review. *ChemSusChem* 4, 1538-1556). This flexibility for different  $H_2/CO$  ratios is of great interest when using syngas derived from biomass or coal gasification, which present  $H_2/CO$  molar ratios lower than 2 (Lappas and Heracleous, 2016). This is related to the high WGS activity of Fe-based catalysts, which could compensate the lack of hydrogen until reaching the stoichiometric proportions required for the FT reaction (Sartipi et al., 2014).

Supported catalysts for FTS have been extensively studied in academia, in spite of only Co-supported catalysts have been used up to know at industrial scale in the LT-FTS (Luque et al., 2012). In this sense, FT catalyst structure and performance are highly influenced by the catalyst support. Conventional inorganic materials such as  $Al_2O_3$ ,  $SiO_2$ ,  $TiO_2$ , and zeolites have been frequently studied to disperse and stabilize both Fe and Co catalyst nanoparticles (Sun et al., 2000; Prieto et al., 2009; Sartipi et al., 2014; Abrokwhah et al., 2019). Unfortunately, highly dispersed cobalt and iron nanoparticles can interact with the metal oxide support during the thermal activation treatments (high-temperature calcination and/or reduction), resulting in formation of cobalt and iron-supported mixed

compounds (i.e., cobalt and iron silicates in the case of Co/ $SiO_2$  and Fe/ $SiO_2$  catalysts, respectively), which are hardly reducible and therefore nonactive in the FTS reaction (Lund and Dumesic, 1981; Tauster et al., 1981; Munirathinam et al., 2018). In order to tackle this issue, the use of more inert materials, such as carbon-containing supports, has been proposed. Carbon-based materials have been reported to minimize the metal-support interactions because of their inert nature, high surface area and tunable porous texture, and surface chemistry. The high thermal conductivity of carbon materials is an additional advantage of carbon-based supports for FTS catalysts, which favors the catalyst heat-transfer properties during the highly exothermic FTS reaction (Chin et al., 2005; Asalieva et al., 2020). Thus, carbon-based materials have been successfully applied as catalyst supports for FTS (Xiong et al., 2010; Moussa et al., 2014; Dlamini et al., 2020), but only in the area of research because they have not yet been used at an industrial level, as it has been already mentioned.

**Figure 1** shows the evolution of the number of research papers published regarding the use of carbon-based materials as catalyst supports for FTS. We have selected for the present work 164 research papers reported in scientific journals of high impact (80% Q1) indexed in JCR in the areas of knowledge of Chemistry, Chemical Engineering, Environmental Engineering, and Materials Technology, between 2004 and 2020. Approximately, 25% of the studies related to catalysts for FTS are devoted to catalyst supported on carbon materials and 35% of these research studies have been reported in the last 3 years, which highlight the potential interest in this topic. Accordingly, 67.3% of the research papers correspond to carbon-supported Co catalysts, 32.7% to Fe-related catalysts, and 2.5% to Ru catalysts. Ru has been less investigated due to the high metal costs and, therefore, to the greatest difficulties of implementation in industrial applications. Furthermore, the most active area of research along the past 2 decades has been in activated carbons (AC, 15%) and in multiwall carbon nanotubes and nanofibers (CNTs and CNFs, respectively, 42%). More recently, there has been an increasing interest in the use of new carbon materials with uniform structures for FTS process, such as ordered mesoporous carbons (OMC), carbon spheres (CS), and graphene. A considerable increasing number of studies have also investigated the use of carbon/oxide hybrid supports (i.e., C/ $Al_2O_3$ , C/ $SiO_2$ , and C/HZSM-5), and, very recently, Metal Organic Frameworks-derived catalysts. In the latter case, the thermal decomposition in inert conditions of Co- and Fe-containing MOFs, namely, the MOF-mediated synthesis technique, resulted in carbon-doped Co and Fe metal catalysts with very interesting results for FTS (Santos et al., 2015; Otun et al., 2020). **Figure 2** summarizes the different carbon support materials reported in the literature for FTS catalysts classified according to the carbon structure and morphology.

Herein, we have summarized the most relevant and recent advances in conversion of syngas to hydrocarbons by FTS using heterogeneous catalysts supported on different carbon-based materials (AC, OMC, CNTs, CNFs, CSs, and graphene) reported during the last 2 decades. We first bring to the attention of the reader important characteristics to take into

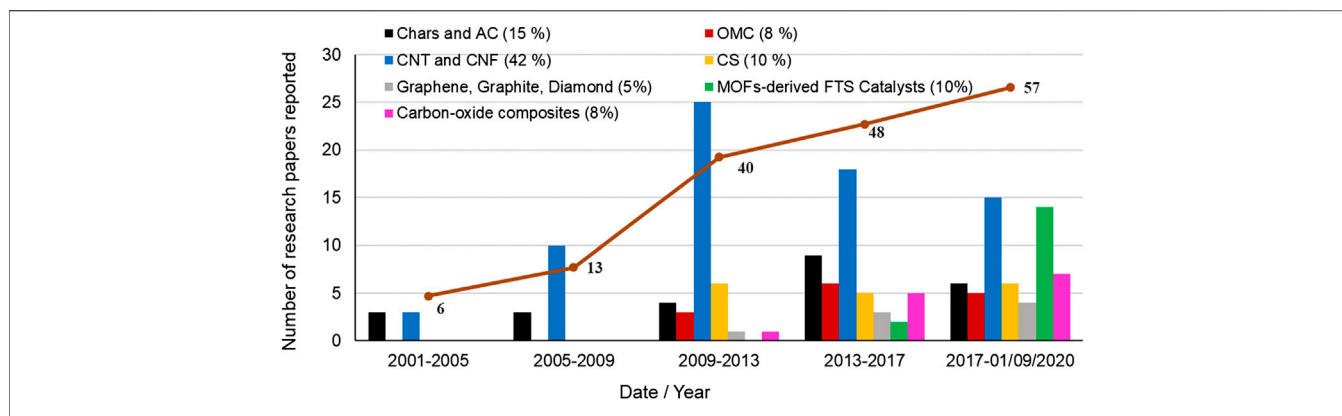


**FIGURE 1** | Evolution of the literature reported for different carbon-based supports for FT catalysts in the last 2 decades. The values in parenthesis in the legend indicate the percentage of research papers dedicated to each carbon support. Source: Scopus.

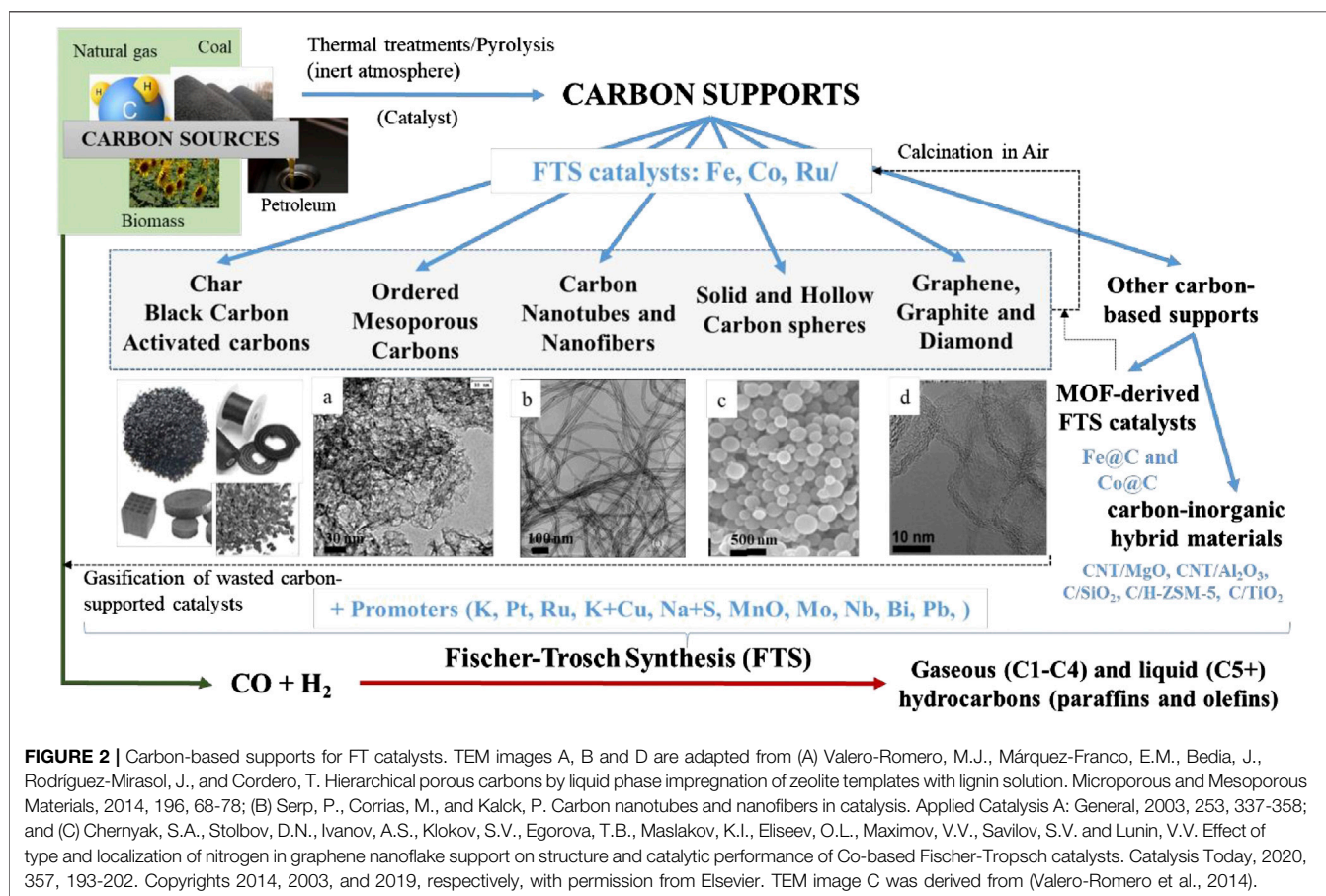
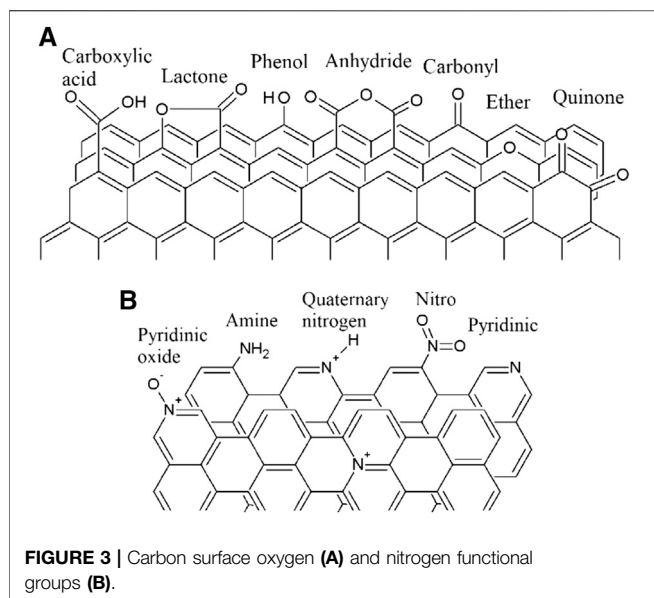


**FIGURE 2** | Carbon-based supports for FT catalysts. TEM images A, B and D are adapted from (A) Valero-Romero, M.J., Márquez-Franco, E.M., Bedia, J., Rodríguez-Mirasol, J., and Cordero, T. Hierarchical porous carbons by liquid phase impregnation of zeolite templates with lignin solution. *Microporous and Mesoporous Materials*, 2014, 196, 68-78; (B) Serp, P., Corrias, M., and Kalck, P. Carbon nanotubes and nanofibers in catalysis. *Applied Catalysis A: General*, 2003, 253, 337-358; and (C) Chernyak, S.A., Stolbov, D.N., Ivanov, A.S., Klovov, S.V., Egorova, T.B., Maslakov, K.I., Eliseev, O.L., Maximov, V.V., Savilov, S.V. and Lunin, V.V. Effect of type and localization of nitrogen in graphene nanoflake support on structure and catalytic performance of Co-based Fischer-Tropsch catalysts. *Catalysis Today*, 2020, 357, 193-202. Copyrights 2014, 2003, and 2019, respectively, with permission from Elsevier. TEM image C was derived from (Valero-Romero et al., 2014).

account in the use of carbon materials in catalysis, particularly for the FTS process. Afterward, the different examples from the literature are thoroughly reviewed and discussed by classifying the carbon-based supports according to their properties, structure, and morphology. Otun et al. (2020) have recently reported a review on the use of MOF-derived catalysts in the FTS process. It is also to be noted that several important reviews have appeared on carbon supports for FTS catalysts in the last decade (Yang et al.,

2011; Xiong et al., 2015; Ahn et al., 2016). However, this review focusses on the general relationship between the carbon catalysts properties, structure, and morphology and the catalytic performance in the FTS process from the most relevant and recent literature, with special emphasis in some catalyst aspects, such as pore structure, carbon support modification (functionalization and doping), catalyst preparation methods, catalyst stability, reducibility, metal particle size, and location



and the use of metal promoters. Furthermore, the FTS catalyst performance in terms of FTS activity (CO conversion, metal-time yield (MTY), and turnover frequency (TOF)) and hydrocarbons selectivity is also tabulated for all the carbon-based supports (**Supplementary Tables S1–S7**), compared and deeply discussed. Finally, in the conclusions, some challenges and future perspectives about the industrial feasibility of carbon-based supported FT catalysts are also considered.

## GENERAL CONSIDERATIONS ABOUT THE USE OF CARBON MATERIALS AS FT CATALYST SUPPORTS

The interest in carbon-based supports for catalytic applications relies on the great advantages it exhibits, such as good thermal conductivity, high specific surface area, and high thermal and chemical stability under middle operation conditions. On the other hand, in the case that biomass or lignocellulosic residues are used as carbon precursors, it would result in an additional advantage from the economic and environmental points of view (Rosas et al., 2010; Moulefera et al., 2020). Another remarkable feature that carbon supports possess is the possibility of tailoring both their porous structure and surface chemistry, not only during the preparation procedure, but also by further modification *via* different chemical and thermal treatments, which allow bonding extra heteroatoms on their surfaces, such as oxygen and nitrogen surface groups (Figueiredo et al., 1999; Xiong et al., 2014b). **Figure 3** shows typical oxygen (**Figure 3A**) and nitrogen surface groups (**Figure 3B**) on the carbon surface. The nature and concentration of functional groups on the surface of carbon materials have a significant influence on the catalyst dispersion and reducibility given that these surface groups act as anchoring sites for the active phase of supported catalysts and even they can be also the active sites for specific

catalytic reactions. Oxygen functional groups are the most important in this context, as they can be formed spontaneously by exposure to the atmosphere or can be further generated or modified by oxidative and/or thermal treatments, in the liquid phase ( $(\text{NH}_4)_2\text{S}_2\text{O}_8$ ,  $\text{HNO}_3$ ,  $\text{H}_2\text{O}_2$ ) (Moreno-Castilla et al., 1995; Moreno-Castilla et al., 2000; Palomo et al., 2017), or in the gas phase ( $\text{O}_2$ ,  $\text{O}_3$ ,  $\text{N}_2\text{O}$ , and  $\text{HNO}_3$  vapor) (Figueiredo et al., 1999; Valero-Romero et al., 2017). Nevertheless, such treatments, particularly those under severe oxidizing conditions, may cause the partial destruction of the pore structure of the carbon material due to their gasification to  $\text{CO}_2$  (and  $\text{CO}$ ).

Regarding the preparation of catalysts for the FTS, it has been reported that metal-support interactions play a crucial role on the activity of the catalysts (Xiong et al., 2015). The main goal of any catalyst support is to enhance metal dispersion, giving rise a higher number of active sites on the catalyst surface as compared to the unsupported catalyst. Due to their inertness nature, especially when they are prepared at high carbonization temperatures, carbon materials produce low interactions with the FT metal-supported catalyst, which was investigated for the first time by Jung et al. (1982). Since then, many publications can be found in the literature on this issue, most of them dealing with the reduction of the metal-support interactions (Hernández Mejía et al., 2018; Van Deelen et al., 2019) and with the possibility of achieving a relatively low metal particle size (Bezemer et al., 2006a). However, these weak metal-support interactions are not always beneficial from the catalytic viewpoint. Metal sintering can also take place under reaction conditions, resulting in the loss of catalytic activity (De Smit and Weckhuysen, 2008). In order to overcome this metal sintering process and to achieve a higher metal dispersion values, several authors studied the modification of the carbon surface with oxygen and nitrogen surface groups, where the FT metal catalyst can be bonded during the impregnation stage (Xiong et al., 2010; Xiong et al., 2014a; Xiong et al., 2014b; Chernyak et al., 2016).

Another important issue relies on the maximum temperature at which carbon supports are stable under the operating conditions required for the FTS process. HT-FTS is usually carried out at  $340^\circ\text{C}$ . However, the conditions for iron/cobalt reduction usually require a higher temperature, above  $350^\circ\text{C}$ , under hydrogen flow (Chen et al., 2018). On this regard, several authors have observed the evolution of methane during the reduction treatment from  $350^\circ\text{C}$  (Bezemer et al., 2006b; Fu et al., 2014b; Valero-Romero et al., 2016). The chemical and thermal stability of a particular carbon-based catalyst depends on several aspects, such as the metal content. Therefore, catalyst stability measurements during reduction for each individual carbon-based catalyst should be addressed in order to determine the optimum reduction temperature.

On the other hand, the use of carbon materials as support of iron catalysts for FTS seems to be beneficial due to the easier formation of iron carbide species, which have been claimed to be the active phases for this reaction (Chen et al., 2008; Wezendonk et al., 2018). On the contrary, the formation of carbides has been reported to be not useful for cobalt FTS catalysts, where the active

**TABLE 1** | Textural parameter range values and metal content range for Fe- and Co-supported carbon catalysts used in FTS.

Carbon support	Co or Fe wt%	S <sub>BET</sub>	Total pore volumen cm <sup>3</sup> /g	Average pore diameter nm
Activated carbons	10–20	476–990	0.29–0.7	1.1–5.4
Ordered mesoporous carbons	10–20	350–1,326	0.48–1.32	2.5–6.8
Carbon nanotubes and nanofibers	10–20	72–255	0.14–0.67	3.4–17.3
Carbon nanofibers	7.5–14.5	169–300	0.29–0.37	4.8–7.6
Carbon spheres (HTC)	5–15.4	350–465	0.21–0.59	2.8–9.1
Graphene	5–15	250–700	0.9–1.5	n.d.

phase is metallic cobalt. In this line, the formation of cobalt carbides has been reported to lower the catalytic performance of FTS catalysts, giving rise to high amounts of methane (Mohandas et al., 2011). However, carbon materials can be used as support of cobalt catalysts if harsh preparation conditions responsible for the formation of cobalt carbides are avoided.

High pore volume and high mean pore size have been reported to be important parameters to control metal particle size and dispersion on carbon materials for the FTS process (Ahn et al., 2016). A carbon support with a well-developed mesoporous and macroporous structure would have excellent advantages in FT reaction, because larger pores benefit the diffusion of the reactants and hydrocarbon products to and from the catalytic active reaction sites, respectively, thus, enhancing the production for longer hydrocarbon chains.

Finally, another interesting issue to take into account when carbon-based supports are used in the FTS process is the possibility of recovering the metal phase after aging or deactivation of the catalytic system under FTS conditions by a simple combustion or gasification of the carbon support. This type of active phase recovering would also result in a negligible net increase of CO<sub>2</sub> to the atmosphere in the case that renewable biomass had been used as the carbon source in the catalyst preparation, contributing to the reduction of greenhouse gas emissions. In addition to this, the spent (aging or deactivated) catalysts and/or mixtures of residual lignocellulosic biomass and spent catalysts could be used as feedstock in the gasification reactor for the production of syngas for the FTS (Figure 2).

## CARBON-BASED MATERIALS USED AS CATALYST SUPPORTS FOR FTS

### Catalysts Supported on Activated Carbons

The earlier studies on carbon-supported catalysts for the FTS process focused on the use of AC, black carbon, and glassy carbon as supports. These works were dedicated to study how to achieve small metal particles, and hence a high metal dispersion, and to study the metal-support interactions (Xiong et al., 2015). In the last years, however, ACs have been mostly studied as model catalyst supports for the FTS reaction, with the purpose of analyzing the effect of the carbon nature and porous texture as compared with other supports and with the aim of analyzing the effect of metal promoters on the FTS catalyst performance.

The preparation of AC can be achieved using several kinds of lignocellulosic waste as carbon precursor and by different chemical and/or physical activation processes, giving rise to carbon materials possessing different porous textures and surface chemistry. In this sense, a particular surface chemistry can be achieved by choosing the proper activation process (Rodríguez-Reinoso and Molina-Sabio, 1992; Rosas et al., 2008; Rosas et al., 2010). According to the literature, most of the ACs used for research as FTS catalyst supports were mainly commercial (purchased), with coconut shell or almond being the most commonly used carbon precursors, and as for the catalyst preparation method, incipient wetness impregnation (IWI) was commonly selected. In general, Co- and Fe-supported AC catalysts were characterized by a high BET surface area and pore volume and by a high contribution of microporosity (pores <2 nm). **Table 1** shows the textural parameter range values of different carbon-supported catalysts for the FTS process from the literature reviewed in the present work, and **Table 2** summarizes the FTS performance for the most relevant Fe- and Co-supported AC catalysts and their metal loading, and when a metal promoter is used, its loading is also shown. In addition to this, further details are reported in the supporting information file (**Supplementary Table S1**) as their metal particle size, C<sub>2</sub>-C<sub>4</sub> olefin/paraffin ratio (O/P), and  $\alpha$  value obtained from FTS.

### Effect of Metal-Support Interactions and Activated Carbon Porous Texture on FTS

Activated carbon has been used as a model catalyst support in order to study the influence of metal-support interactions on the FTS catalyst performance. In this line, Cheng et al. (2014) studied the preparation of iron catalyst supported on silica and on different carbon-based materials.  $\alpha$ -Fe<sub>2</sub>O<sub>3</sub> was the main iron phase on silica supports, whereas magnetite (Fe<sub>3</sub>O<sub>4</sub>) and/or maghemite ( $\gamma$ -Fe<sub>2</sub>O<sub>3</sub>) were mainly present on the carbon supports. The presence of partially reduced iron oxides was related to the carboreduction of iron oxides during the iron nitrate precursor decomposition stage. These authors also found a higher carburization extent for the carbon-based iron catalysts as compared to the silica-supported counterparts during a CO activation stage. The higher activity found for the carbon-supported catalysts was attributed to the presence of iron carbide-magnetite composites. Among the carbon-based catalysts, the one prepared using AC as support presented the second highest

**TABLE 2** | Summary of FTS performance of cobalt and iron catalysts supported on AC.

No.	Catalyst	Co or Fe wt%	Promoter wt%	T °C	P bar	H <sub>2</sub> /CO	SV m <sup>3</sup> kg <sub>cat</sub> <sup>-1</sup> h <sup>-1</sup>	MTY <sup>a</sup>	TOF <sub>10-3</sub> s <sup>-1</sup>	X <sub>CO</sub> %	S/ %			Ref.
											C <sub>1</sub>	C <sub>2-4</sub>	C <sub>5+</sub>	
1	Fe/AC	10	n.d. <sup>b</sup>	300	20	2.1	16	43.97	n.d.	64	7.8	38.5	53.7	Cheng et al., (2014)
2	15.7Fe/AC	15.7	n.d.	300	20.68	0.9	3	n.d.	n.d.	96.9	34.4	19.1	16.5	Ma et al., (2007)
3	15.7Fe/0.9K/AC	15.7	0.9	280	20.68	0.9	3	n.d.	n.d.	85.7	8.6	34.9	56.5	Ma et al. (2007)
4	Kn/Fe/AC	12.5	1.06	240	20	2	16	25.57	n.d.	62	9.2	18.8	72.1	hernavskii et al. (2018)
5	Fe/Kn/AC	8.5	0.9	240	20	2	16	52.88	n.d.	87.2	9.7	20	70.3	Chemavskii et al., (2018)
6	15Co/AC	15	0	230	20	2	0.5	n.d.	n.d.	29.7	25	14.6	60.4	Chen et al. (2012)
7	15Co/MC	15	0	230	20	2	0.5	n.d.	9.4	73.1	19.1	10.1	70.8	Chen et al. (2012)
8	4Zr-10Co/AC	12.5	Zr: 4	250	25	2	500 h <sup>-1</sup>	n.d.	n.d.	86.4	14.2	14.8	71	Wang et al. (2008)
9	0.2La4Zr-10Co/AC	14	Zr: 4 La: 0.2	250	25	2	500 h <sup>-1</sup>	n.d.	n.d.	92.3	11.5	13.8	74.7	Wang et al. (2008)
10	30Co/AC-2	30	n.d.	260	5	2	8	n.d.	n.d.	100	54.4	20.7	24	Jiang et al. (2020)
11	30Co0.4Na/AC-2	30	0.4	260	5	2	8	n.d.	n.d.	98.7	49.9	16	34.1	Jiang et al. (2020)
12	30Co10Mn/AC-2	30	10	260	5	2	8	n.d.	n.d.	83.3	15.3	20.7	63.9	Jiang et al. (2020)
13	30Co10Mn0.4Na/AC-2	30	Mn: 10 Na:0.4	260	5	2	8	n.d.	n.d.	73.8	14.2	28.4	57.4	Jiang et al. (2020)

<sup>a</sup>Metal-time yield ( $10^{-5} \text{ mol}_{\text{CO}} \text{ g}_{\text{Co,Fe}}^{-1} \text{ s}^{-1}$ ).

<sup>b</sup>n.d.: not determined.

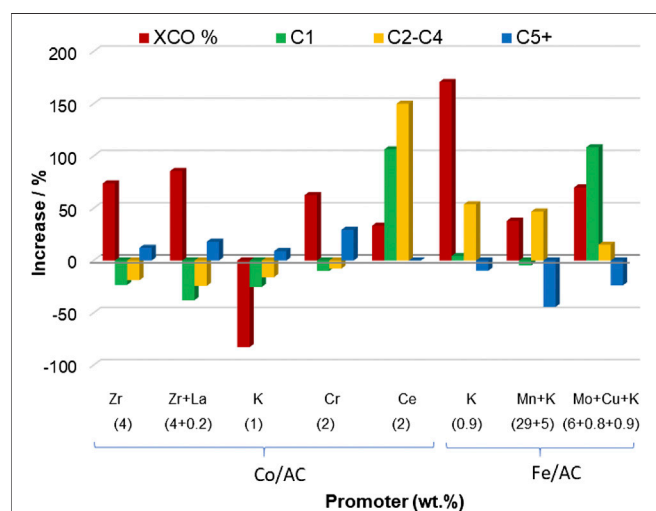


**FIGURE 4** | Increase in CO conversion (except for Ce and Mo+Cu+K, that is syngas conversion) and in selectivity to C<sub>1</sub>, C<sub>2</sub>-C<sub>4</sub>, and C<sub>5+</sub> hydrocarbons values for different promoted Co/AC and Fe/AC catalysts compared to the ones of the unpromoted counterpart. The title in the x-axis indicates the promoter and its concentration in wt%. Data are adapted from refs. (Ma et al., 2004; Ma et al., 2006; Ma et al., 2007; Wang et al., 2008; Chen et al., 2012; Tian et al., 2017; Zhao et al., 2019). Reaction conditions: Zr and Zr+La, 250°C, 25 bar, H<sub>2</sub>/CO = 2, 500 h<sup>-1</sup>; K, 230°C, 20 bar, H<sub>2</sub>/CO = 2, 0.5 m<sup>3</sup> kg<sup>-1</sup> h<sup>-1</sup>; Cr, 220°C, 30 bar, H<sub>2</sub>/CO = 2, 2,000 h<sup>-1</sup>; Ce, 240°C, 24 bar, H<sub>2</sub>/CO = 2, 650 h<sup>-1</sup>; K, 280°C, 20 bar, H<sub>2</sub>/CO = 0.9, 3 m<sup>3</sup> kg<sup>-1</sup> h<sup>-1</sup>; Mn+K, 320°C, 20 bar, H<sub>2</sub>/CO = 1, 3,000 h<sup>-1</sup>; and Mo+Cu+K, 320°C, 20 bar, H<sub>2</sub>/CO = 0.9, 3 m<sup>3</sup> kg<sup>-1</sup> h<sup>-1</sup>.

activity, being only surpassed by the one prepared using carbon nanotubes as support. The Fe/AC catalyst showed a CO conversion of 64%, with high selectivity to C<sub>5+</sub> hydrocarbons (53.7%) (entry 1, Table 2) and a relatively high O/P ratio, 1.2. Similar conclusions were found by Jiang et al. (2017), who also compared the preparation of iron catalysts on ACs and different inorganic supports.

Fischer-Tropsch reaction is structure sensitive, being the conversion and the product distribution affected by the particle size of the active phase and by the porous texture of the support. On this issue, Fu et al. (2014b) studied the effect of pore size on the activity of cobalt-based catalysts supported on ACs and CNTs for FTS. The extent of reduction of Co/AC catalyst was the lowest, presumably due to the higher metal-support interactions, which gave rise to the lowest CO conversion value. In addition, this catalyst presented the highest and the lowest selectivity to methane and to C<sub>5+</sub>, respectively. These catalytic features were justified based on the presence of a narrow microporosity and a low cobalt particle size, which resulted into a higher diffusion rate for H<sub>2</sub> as compared to CO, resulting in a high H<sub>2</sub>/CO ratio inside the pores. Likewise, Chen et al. (2012) compared two AC supports with different average pore sizes (5.2 vs 2.5 nm). The catalytic results were in line with the findings reported by Fu et al. (2014b). The mesoporous carbon-based catalyst (15Co/MC) presented more than twice the CO conversion value than the one of the microporous carbon-based catalyst (15Co/AC), 73.1% vs 29.7%, respectively (entries 6 and 7, Table 2). In addition, the former presented a higher selectivity to C<sub>5+</sub> hydrocarbons and a lower selectivity to methane.

### Effect of Metal Promoters on FTS

The most commonly used promoters for Fe/AC catalysts are K, Mn, and Mo. On the other hand, K, Zr, Ce, Cr, Na, and Mn have been studied as catalyst promoters for Co/AC catalysts. Figure 4 represents the increase in the CO conversion and selectivity to the main reaction products values for some Co- and Fe-supported catalyst on AC in comparison with those for the unpromoted counterpart.

### Effect of Promoters in Iron-Based Catalysts

Some authors have reported an enhancement of CO conversion under certain K promotion amounts in Fe/AC catalysts. For

example, Ma et al. (2007) observed that a K content of 0.9 wt% produced an improvement of CO conversion as compared to the unpromoted catalyst (entries 2 and 3, **Table 2**). The selectivity to CO<sub>2</sub> was also increased with K promotion, due to the enhancement effect of K over the WGS reaction. Additionally, methane selectivity was reduced, whereas longer chain hydrocarbons were formed. Furthermore, the O/P ratio was also increased from 0.1 to 5 for C<sub>2</sub>-C<sub>4</sub> short hydrocarbons. In this line, Chernavskii et al. (2018) observed that the catalyst prepared by first loading iron and then potassium as promoter showed a CO conversion value of 62%. However, when following a reverse sequence order for metal deposition (first K, then Fe), the CO conversion value reached a value of 87.2% (entries 4 and 5, **Table 2**). These differences in CO conversion were attributed to the magnetite particle size formed in each catalyst. The authors claimed that the alkalization of the AC, prior to iron impregnation, increased the number of oxygen-containing groups on the AC surface, giving rise to the formation of more nucleation centers for Fe<sup>3+</sup> ions and consequently, smaller magnetite particles were formed when K was firstly loaded on the AC.

Ma et al. (2006) studied the effect of Mo loading (6 and 12 wt%) on the properties and the catalytic performance of Fe-Cu-K-supported AC catalysts. The addition of Mo significantly inhibited iron reduction, which was attributed to the existence of iron-molybdenum mixed oxides, which were more difficult to reduce. Promotion with 6 wt% Mo showed a lower initial syngas conversion value (58%), which increased with time-on-stream up to 81% and remained unaltered for more than 80 h, which was attributed to the Mo capability of inhibiting iron sintering (Zhao et al., 1994). The addition of Mo also increased the selectivity to methane and C<sub>2</sub>-C<sub>4</sub> hydrocarbons, lowered the selectivity to C<sub>5+</sub>, and reduced the O/P ratio (**Figure 4**).

Tian et al. (2017) studied the effect of Mn as promoter for Fe/AC catalysts. Prior to iron impregnation, the AC support was oxidized with KMnO<sub>4</sub>. During the KMnO<sub>4</sub> treatment, a redox reaction between the carbon surface and the KMnO<sub>4</sub> occurred, yielding a uniform MnO<sub>2</sub> layer covering the surface of the AC-oxygenated surface groups. Additionally, K was deposited on the carbon surface. The presence of K and Mn in the catalysts resulted in an enhancement of the CO conversion value (37%, with respect to that of the unpromoted catalyst) (**Figure 4**). Furthermore, the selectivity to main reaction products were also affected by the promoters, being observed an increase of a 46% in the C<sub>2</sub>-C<sub>4</sub> selectivity and a decrease of a 44% in the C<sub>5+</sub> selectivity, with respect to those of the unpromoted catalyst. In addition, the O/P ratio outstandingly increased from 0.65 for the unpromoted catalyst to 4.88 for the promoted one. The promotion effect of Mn was associated to the synergistic effect of MnO and Hägg carbides in enhancing CO adsorption and dissociation and K helped to form iron carbides on the AC surface.

In summing up, K promotion of Fe-based catalysts resulted in the increase of the CO conversion, when it was loaded in certain controlled amounts, and an enhancement of the activity for WGS. Additionally, the olefin/paraffin ratio and the C<sub>5+</sub> selectivity values were increased. Mn and K promotion enhanced the CO

conversion value and gave rise to a higher C<sub>2</sub>-C<sub>4</sub> olefin production. On the other hand, the addition of Mo as a promoter has been shown to lower the initial activity but also to enhance the catalyst stability.

### *Effect of Promoters in Cobalt-Based Catalysts*

Ma et al. (2004) studied the effect of Zr, K, and Ce as promoters for Co/AC catalysts. K acted as a strong poison for the catalyst, decreasing syngas conversion and methane selectivity, as compared to the unpromoted catalyst (**Figure 4**), which was attributed to the possible coverage of cobalt active sites by K. On the contrary, both Zr and Ce had a positive impact in the catalytic activity. Zr promoted CO conversion without largely modifying the hydrocarbon selectivity values and the activity for WGS. Ce enhanced both syngas conversion and activity for WGS and increased the methane and C<sub>2</sub>-C<sub>4</sub> selectivity values. The positive effects of Zr and Ce as promoters were attributed to the improvements found in cobalt dispersion and to the enhanced interaction between cobalt and the oxygen surface groups resulting from the addition of Zr and Ce to the AC.

Based on these results, Wang et al. (2008) conducted an in-depth research focused on studying the effect of lanthanum in Zr-promoted Co/AC catalysts. The active phase of the catalysts was composed by 10 wt% Co, 4 wt% Zr, and different amounts of La. The presence of La in the catalyst increased the cobalt reducibility at low La loadings. However, La was detrimental at higher loadings. The CO conversion value increased from 86.4 to 92.3% when the content of La increased from 0 to 0.2% (entries 8 and 9, **Table 2**) and the C<sub>5+</sub> selectivity was higher compared to the unpromoted catalyst.

Promotion of Co/AC catalysts with Cr (0–5wt%) resulted in the reduction of the cobalt species crystal size, excepting for the highest Cr content (Zhao et al., 2019). Additionally, the extent of reduction of the catalyst was also enhanced by the presence of Cr. Structural analyses of the active sites showed that the presence of Cr suppressed the formation of cobalt carbides. The reaction results showed an increase in both the CO conversion and the selectivity to C<sub>5+</sub> values for a Cr content of 2% (**Figure 4**). Furthermore, the O/P ratio was lower after Cr promotion. The authors attributed these catalytic features to the higher H<sub>2</sub>-rich surface environment caused by Cr promotion in the catalyst, which facilitated the  $\alpha$ -hydrogen addition step and suppressed the  $\beta$ -hydride elimination and CO insertion steps, simultaneously.

Jiang et al. (2020) studied the promotion effect of Mn and Na on Co/AC catalysts. The unpromoted catalyst showed a CO conversion of 100% with a very high selectivity to methane (54.4%). Na promotion slightly decreased the CO conversion and methane selectivity values (98.7 and 49.9%, respectively). On the other hand, the presence of Mn slightly decreased the CO conversion value to 83.3% and noticeably the methane selectivity to 15.3%. The simultaneous presence of Mn and Na in the catalyst further reduced the CO conversion value from 83.3 to 73.8% as compared to the one for the catalyst just promoted with Mn (entries 10–13, **Table 2**). Furthermore, the O/P ratio experienced a noticeable increase, from 0.65 for the catalyst promoted with Mn to 1.54, when using together Na and Mn as promoters. Another feature observed in this work was the

capacity of Na to enhance the WGS reaction activity in cobalt catalysts.

## Catalysts Supported on Ordered Mesoporous Carbons

The presence of narrow micropores in ACs resulted in internal diffusion limitations for reagents and products when they were used as catalyst supports for the FT process (Chen et al., 2012; Fu et al., 2013; Fu et al., 2014b). To overcome this problem, the use of carbons with a wider porous structure, such as ordered mesoporous carbons (OMCs), has been studied. Co and Fe supported on OMCs are characterized by exhibiting an ordered and well-defined mesoporous texture, with a large pore volume and average pore diameter in the range of 2–6 nm (Table 1). The preparation of OMCs can be carried out by two approaches: (1) the hard-template method, in which an inorganic material, such as SBA-15, is used as template of a carbon source, and then it is removed by HF/NaOH treatments. (2) The soft-template method, so-called solvent induced self-assembly (EISA), which involves the use of an organic directing agent, such as Pluoric F127. In this case, the template is removed during the carbonization step. **Supplementary Table S2** summarizes the FTS performance for the most relevant Fe and Co/OMC catalysts.

### Effect of the OMC Preparation: The Hard-Template Method

Knox et al. (1986) were pioneers in reporting the preparation of OMCs by the hard-template method. Among the reported OMC, CMK-3, a hexagonally structured OMC, is the most commonly used OMC support for FTS catalysts. This material was first synthesized by Jun et al. (2000), using SBA-15 as the hard template and sucrose and H<sub>2</sub>SO<sub>4</sub> in water solution as the carbon source.

For example, Oschatz et al. (2016b) prepared OMC-supported iron catalysts, using CMK-3. The active phase (Fe, Na, and S) loading was carried out by IWI. Afterward, the catalysts were stabilized at different temperatures. Hematite nanoparticles were found for calcination temperatures up to 500°C. Above this temperature, iron carbide species and metallic iron were found. Additionally, iron particles wrapped by a graphite shell forming core-shell structures were found at temperatures above 800°C, which lowered the catalytic activity. The lowest selectivity to methane and the highest selectivity to C<sub>2</sub>–C<sub>4</sub>, 13.4 and 59.5%, respectively, were achieved for the catalyst carbonized at 500°C (entry 1, **Supplementary Table S2**). An outstanding O/P ratio value of 10 was attributed to the efficient promotion of the catalyst with S.

Likewise, Kang et al. (2017) studied the preparation of iron catalyst for FTS using CMK-3 as support. In this case, metal loading was carried out by directly grounding the CMK-3 support with iron nitrate (in a physical mixture). The catalyst was stabilized under CO atmosphere. Uniformly distributed Fe<sub>5</sub>C<sub>2</sub> nanoparticles were found in the pore system of the CMK-3. After a long induction period, the catalyst reached a 91.4% steady-state CO conversion value. The product distribution remained

unaltered during the induction period, showing selectivity values to CH<sub>4</sub>, C<sub>2</sub>–C<sub>4</sub>, and C<sub>5+</sub> of 23.3, 68.3, and 8.3%, respectively (entry 2, **Supplementary Table S2**).

Co-supported CMK-3 catalysts were also studied by Fu et al. (2013) and Li et al. (2019). The loading of cobalt (20%) was carried out by ultrasonication-assisted IWI followed by stabilization at 200°C (Fu et al., 2013) and 350°C (Li et al., 2019). The average pore size of the catalyst was smaller for the sample treated at the highest temperature. However, similar CoO<sub>x</sub> crystallite sizes were found for both catalysts. The CO conversion values were also very similar for both catalysts. Nevertheless, the catalyst carbonized at 200°C (Fu et al., 2013) yielded a higher production of diesel range hydrocarbons than gasoline ones, 48 vs 35%, whereas the catalyst stabilized at 350°C (Li et al., 2019) presented a higher selectivity to hydrocarbons in the gasoline range (entries 10 and 11, **Supplementary Table S2**).

Zhao et al. (2020) studied the preparation of OMC-supported cobalt catalysts. In this case, for the preparation of the OMC support, SBA-16 was used as the hard template and furfuryl alcohol (FA) and oxalic acid in ethanol solution were used as carbon source. After a carbonization stage, HF was used to eliminate the silica template and cobalt loading was carried out by IWI using cobalt nitrate. The CoO crystallite size slightly increased with increasing the support carbonization temperature due to the diminishment of the metal-support interactions. The catalyst presenting the highest catalytic activity was the one prepared using the OMC carbonized at the highest temperature (1,300°C), due to lower cobalt support-interactions and higher reducibility of the cobalt species. This catalyst showed a CO conversion value of 49.7% and a selectivity to C<sub>5+</sub> hydrocarbons of 74% (entry 12, **Supplementary Table S2**).

### Effect of the OMC Preparation: The Soft-Template Method

Liu et al. (2017) studied the preparation of OMC-based cobalt FTS catalysts in a single step using Pluoric F127 as directing agent, resorcinol and formaldehyde as carbon sources, and cobalt nitrate as metal precursor. FTS experiments showed a CO conversion value of 30.2%, with selectivity values to methane and to C<sub>5+</sub> hydrocarbons of 15.2 and 81.5%, respectively (entry 13, **Supplementary Table S2**). The catalytic activity reported in this study is lower than those reported by other studies working under similar operation conditions (Fu et al., 2013; Li et al., 2019; Zhao et al., 2020). A possible explanation to this lower catalytic performance reported by Liu et al. (2017) could be the relatively high cobalt particle size and the lack of accessibility to these cobalt particles due to the deep embedment in the carbon support during the synthesis procedure.

### Tailoring OMC Supports for Controlling Metal Crystallite Size

Metal particle size is a highly important Fischer–Tropsch catalyst feature, and thus, different catalyst synthesis strategies have been proposed to control the size of the active phase on OMC supports.

Yang et al. (2012) carried out a study dedicated to control the cobalt particle size in OMC-supported FTS catalysts by the modification of the OCM synthesis procedure. For this aim, different amounts of FA (carbon source) were introduced in

SBA-15 (hard template). Cobalt loading was carried out by IWI using cobalt nitrate. The average size of the cobalt particles on the catalyst increased with increasing the FA content. Additionally, the allocation of the cobalt particles was shifted to the outer surface when increasing the FA content. The highest activity was achieved for the catalysts prepared using a 50% FA (CO conversion value of 45.07%, with methane, C<sub>2</sub>-C<sub>4</sub>, and C<sub>5+</sub> selectivity values of 24.6%, 11.31%, and 64.09%, respectively), entry 14, **Supplementary Table S2**.

More recently, Yang et al. (2014) carried out a study to control the cobalt particle size of FTS catalysts using an N-doped OMC as catalyst support. Nitrogen incorporation was carried out by a postsynthetic route using cyanamide. The metal loading was carried out by IWI using cobalt nitrate in acetone solution. The authors found that the higher the N content in the support, the smaller the cobalt particle size. This fact was associated to the capacity of N of improving dispersion of cobalt metal species and forming more uniform particles. The TOF values and the catalytic activity increased with increasing the cobalt particle size up to a 10 nm. Above this value, the TOF remained constant, but a decrease in the catalytic activity was observed.

Likewise, Sun et al. (2012) investigated the preparation of OMC-supported catalysts with different iron crystallite sizes for the FTS reaction. The preparation of the OMC-based catalysts was carried out using Pluronic F127 as directing agent, resol as carbon source, and iron nitrate as metal precursor. Different amounts of a chelating agent, acetylacetone, were used with the aim of controlling the metal particle size. The iron particle sizes were reduced when increasing the acetylacetone content. The catalyst presenting the smallest iron particle size (8.3 nm) showed the highest CO conversion value (90.1%), with a low selectivity to CO<sub>2</sub> (13.3%) and very high selectivity to C<sub>5+</sub> hydrocarbons (>68%) (entry 3, **Supplementary Table S2**).

Cheng et al. (2014) controlled the iron particle size by varying solvent (water or acetone) used for the metal impregnation process. The catalyst prepared using water as iron nitrate solvent showed an average crystallite size four times larger than the one prepared using ethanol as solvent. The catalytic results were in line with those reported by Sun et al. (2012), being observed a higher CO conversion for the catalyst presenting a smaller iron particle size (49.7% and 38.5% for the catalysts prepared with ethanol and water, as impregnation solvent, respectively), entries 4 and 5, **Supplementary Table S2**.

### Effect of Metal Promoters on FTS

The use of promoter has been also studied in OMC-supported Fischer-Tropsch catalysts. Cheng et al. (2015) reported that the use of Na as catalyst promoter reduced the average iron phase crystallite size. The reaction results showed that the presence of Na reduced the CO conversion value. However, a selectivity to C<sub>5+</sub> up to 78.9% was obtained for a Na to Fe molar ratio of 0.3 (entries 6 and 7, **Supplementary Table S2**). Na promotion also increased the C<sub>2</sub>-C<sub>4</sub> O/P ratio more than five times the value of the unpromoted catalyst. Similarly, Oschatz et al. (2016a) studied the effect of Na and S as promoters on Fe/OMC catalysts. The reaction results showed that CO conversion was lower for the Na-promoted catalyst than for the Na-S-promoted one. Additionally,

the simultaneous presence of Na and S enhanced the selectivity to C<sub>2</sub>-C<sub>4</sub> as compared to that of the Na-promoted catalyst (entries 8 and 9, **Supplementary Table S2**). The O/P ratio showed an outstanding value of 10 in both promoted catalysts studied.

### Catalysts Supported on Carbon Nanotubes and Carbon Nanofibers

Typically, multiwall carbon nanotubes or carbon nanotubes (MWCNTs or CNTs) and carbon nanofibers (CNFs) are grown by the decomposition of carbon-containing compounds on a metal catalyst particle. By modifying the carbon source, as well as the chemical composition and morphology of the catalyst, it is possible to synthesize CNTs and CNFs with variable crystallinity degrees, sizes, and shapes. The main difference between nanotubes and nanofibers consists in the presence of a hollow cavity for CNTs. Single-wall carbon nanotubes (SWCNTs) are ideally made of a perfect graphene sheet rolled up into a cylinder and closed by two caps (semifullerenes), whereas MWCNTs are formed by concentric SWCNTs with increasing diameter. On the other hand, CNFs are made of domains of sp<sup>3</sup> carbon atoms (graphene-like layers) bounded by sp<sup>3</sup> carbons or other terminal atoms or groups of atoms (Serp et al., 2003).

Typically, Co- and Fe-supported CNTs used in FTS have total surface areas ranging between 70 and 255 m<sup>2</sup>/g (**Table 1**). The pores in these structures can vary from inner hollow cavities with diameters within the micropore range (less than 2 nm) and mesopore range (between 3 and 6 nm) to aggregated pores (>15 and up to 40 nm) in a larger extent, which are formed by interaction of isolated MWCNTs. The length of these structures can range from few microns to several millimeters. Furthermore, the external diameter of the MWCNT can reach 100 nm (Yang et al., 2001). In the case of Co- and Fe-supported CNFs, the surface area can range between 170 and 300 m<sup>2</sup>/g, no micropores are found, and the mesopore volume ranges between 0.5 and 2 cm<sup>3</sup>/g (De Jong and Geus, 2000). The external diameters of CNF are generally higher than the ones presented by nanotubes and can reach 500 nm (Serp et al., 2003). The detailed similarities and differences in adsorption, electronic, thermal, and mechanical properties, and growth mechanisms of CNTs and CNFs have been extensively reviewed (De Jong and Geus, 2000; Serp et al., 2003; Lehman et al., 2011).

Given that CNTs and CNFs are relatively inert materials, it is necessary to modify their nature by introducing surface functional groups in order to attain high stabilization and dispersion of the metal particles on their surface. In addition to this, these materials have been considered as model supports in the FTS reaction process. Therefore, the effect of CNT and CNF functionalization, catalyst preparation methods, metal particle size, pore size, pore confinement, and the incorporation of metal promoters on the catalysts structure and FTS performance have been investigated.

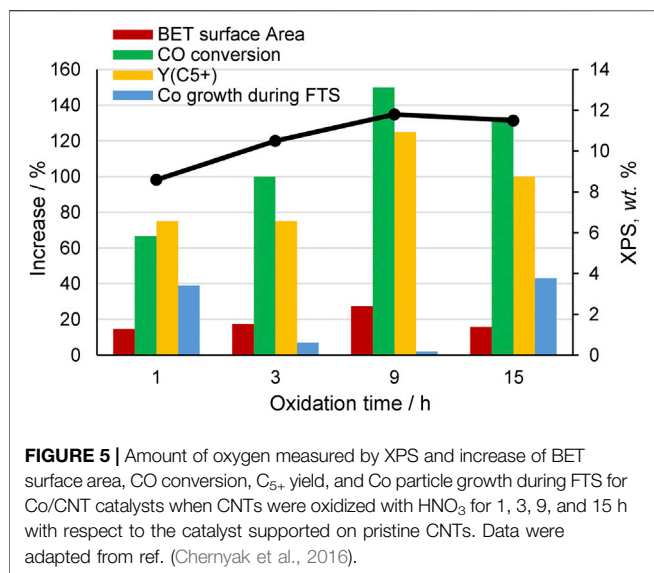
### Effect of CNT and CNF Functionalization and Thermal Treatments

Several studies have been dedicated to study the surface functionalization of CNTs either by introduction of oxygen or

**TABLE 3** | FT performance of unpromoted Co and Fe catalysts supported on CNTs and CNFs after different catalyst preparation methods.

No.	Catalyst	Catalyst preparation method	Co or Fe wt%	T°C	P bar	H <sub>2</sub> /CO m <sup>3</sup> kg <sub>cat</sub> <sup>-1</sup> h <sup>-1</sup>	SV	MTY <sup>a</sup>	TOF 10 <sup>-3</sup> s <sup>-1</sup>	X <sub>CO</sub> %	S/ % C <sub>1</sub> C <sub>2-4</sub> C <sub>5+</sub>				Ref.
1	IWN13	IWI, water	13	210	35	2	n.d. <sup>c</sup>	4.35	22.5	66	n.d.	n.d.	81.7	Bezemer et al. (2006a)	
2	IEN8	IWI, ethanol	7.5	210	35	2	n.d.	3.7	13.5	65	n.d.	n.d.	76.1	Bezemer et al. (2006a)	
3	Co/CNT-IM	IWI	13.2	225	8	2	3,840 h <sup>-1</sup>	n.d.	n.d.	25.9	30.6	n.d.	62.1	Xiong et al. (2011)	
4	Co/CNT-DP	HDP	4.3	225	8	2	3,842 h <sup>-1</sup>	n.d.	n.d.	9.9	23.5	4.4	72.1	Xiong et al. (2011)	
5	Co/CNT-IWI	IWI	17.65	200	10	2	1,066 h <sup>-1</sup>	n.d.	n.d.	65	30.5	22.5	45	Almkhelfe et al. (2018)	
6	Co/CNT-F	Fenton	15.7	200	10	2	1,066 h <sup>-1</sup>	n.d.	n.d.	80	9.4	18.4	70.2	Almkhelfe et al. (2018)	
7	cs_Co <sup>100</sup> /CNT	Colloidal synthesis	10	220	1	2	2002 h <sup>-1</sup>	4.85	n.d.	2.47	39.5	34.5	26	Ismail et al. (2019)	
8	ci_Co <sup>100</sup> /CNT	IWI	10	220	1	2	2003 h <sup>-1</sup>	4.22	n.d.	1.47	37	27	36	Ismail et al. (2019)	
9	Co800	IWI-TT-800°C <sup>b</sup>	10.7	240	20	2	5	11.6	100	66.7	28.9	n.d.	61	Chernyak et al. (2020)	
10	Co/RCR	Reduction-carburization-reduction	8.3	220	10	2	2	0.32	n.d.	n.d.	4.3	2.6	93.2	Ghogia et al. (2020)	
11	hcp-Co/CNF	Thermal decomposition	6.2	220	10	2	2	0.67	5.3	n.d.	3.9	2.3	93.8	Ghogia et al. (2020)	
12	fcc-Co/CNF	Thermal decomposition	8.3	220	10	2	2	0.53	3.4	n.d.	5	2.7	92.3	Ghogia et al. (2020)	
14	Fe/CNT-IW	IWI	12.1	270	8	2	2,120 h <sup>-1</sup>	37.2	n.d.	80	14.6	42.1	43.3	Bahome et al. (2005)	
15	Fe/CNT-DPU	HDP (urea)	10.5	270	8	2	2,120 h <sup>-1</sup>	46.9	n.d.	76.7	15.4	39.8	44.7	Bahome et al. (2005)	
16	Fe/CNT-IWI	IWI	18.47	250	10	2	1,066 h <sup>-1</sup>	n.d.	n.d.	57	42	10	37.5	Almkhelfe et al. (2018)	
17	Fe/CNT-F	Fenton	16.35	250	10	2	1,066 h <sup>-1</sup>	n.d.	n.d.	68	12.5	21.6	62.9	Almkhelfe et al. (2018)	
18	Fe800	IWI-TT-800°C <sup>b</sup>	10.4	300	20	1	5	20.3	0.9	71.4	6.2	10.3	57.3	Chernyak et al. (2020)	
19	Fe-in-CNT	WI	10	270	51	2	20	n.d.	n.d.	40	12	41	29	Chen et al. (2008)	
20	Fe-out-CNT	WI	10	270	51	2	20	n.d.	n.d.	29	15	54	19	Chen et al. (2008)	
21	Fe/CNT-in	IWI	10.2	350	20	1	17	28	436	14.4	34.2	50.8	15	Gu et al. (2019)	
21	Fe/CNT-out	IWI	10.3	350	20	1	17	16	403	24.8	28.5	50.7	20.8	Gu et al. (2019)	

<sup>a</sup>Metal-time yield (10<sup>-5</sup> mol<sub>CO</sub> g<sub>Co,Fe</sub><sup>-1</sup> s<sup>-1</sup>).<sup>b</sup>Thermal treatment in inert conditions (TT).<sup>c</sup>n.d.: not determined.



nitrogen surface groups and the influence of these groups on the structure and the catalytic performance of CNF- and CNT-supported FT catalysts. **Table S3** summarizes the most relevant results regarding the FT performance of unpromoted Co and Fe catalysts supported on CNTs and CNFs after different functionalization pretreatment conditions. In most cases, the optimum catalyst observed from each study is tabulated when different oxidizing conditions are studied. For example, Chernyak et al. (2016) investigated the CNT oxidation prior to Co impregnation by a treatment with  $\sim 70$  wt% HNO<sub>3</sub> for different reaction times and tested them in FTS at 190°C, 1 bar, H<sub>2</sub>/CO of 2 and space velocity (SV) of 2.2 m<sup>3</sup>kg<sub>cat</sub><sup>-1</sup>h<sup>-1</sup>. **Figure 5** compares the results of the cobalt catalyst pretreated in acid for 1, 3, 9, and 15 h with respect to the untreated Co/CNT catalyst. Optimal oxidation conditions were found after 9 h of acid reaction, resulting in Co/CNTs with the highest porous development, oxygen content, and an optimal cobalt particle size of 4.2 nm was obtained after catalyst impregnation and activation, which also presented the highest FTS activity, C<sub>5+</sub> hydrocarbons yield, and lower Co sintering during FTS. These results are in line with the research of Trépanier et al. (2009b) who investigated different nitric acid pretreatment temperatures (entries 1–3, **Supplementary Table S3**). The most severe acid-treatment conditions (15 h) produced the deterioration of the CNT material, resulting in a significant decrease of the BET surface area, which is in line with other studies (Fu et al., 2014a; Nakhaei Pour et al., 2018). The catalytic activity was also maximized for Co and Ru catalysts supported on oxidized CNTs with optimal HNO<sub>3</sub> concentrations of 70 and 68 wt%, respectively (Kang et al., 2009; Vosoughi et al., 2016) (entries 5 and 14, **Supplementary Table S3**). Likewise, pretreatment of CNTs with H<sub>2</sub>O<sub>2</sub> (Nakhaei Pour et al., 2018) and H<sub>2</sub>O<sub>2</sub> + O<sub>3</sub> (Karimi et al., 2014) yielded Co/CNT catalysts with higher FTS activity, higher selectivity to C<sub>5+</sub> hydrocarbon fraction, and high stability compared to the untreated catalyst. Optimal preparation conditions were investigated for oxidizing CNTs for cobalt

catalyst preparation with H<sub>2</sub>O<sub>2</sub> and sonicated *via* a pulsing method (entry 6, **Supplementary Table S3**) (Nakhaei Pour et al., 2018). It appeared that sonication in a short time (10 s) resulted in Co/FCNTs-10 catalyst with a remarkably narrow cobalt particle size distribution.

On the other hand, Eschemann et al. (2015) reported that CNT oxidation adversely influenced the FT performance of the Co/CNT catalysts, with significantly lower cobalt-time yields (CoTYs) and C<sub>5+</sub> selectivity for the cobalt catalyst pretreated in acid for LT-FTS. They ascribed the different catalytic performance to an increase in hexagonal-close-packed crystal structured (hcp-Co) on pristine CNTs compared to the surface-oxidized CNTs. Hcp-Co phase has been experimentally confirmed to be more active and selective to C<sub>5+</sub> than the cubic Ghogia et al. (2020). Likewise, more recently, Van Deelen et al. (2020) reported a negative effect on the catalytic performance of presynthesized 6 nm colloidal CoO nanocrystals supported on oxidized CNTs tested under similar FTS conditions (entries 10 and 11, **Supplementary Table S3**). The different catalytic performance was ascribed to the low crystalline metallic Co content on oxidized CNTs than on pristine CNTs.

In addition, it has been reported that the nature of oxygen functional groups on CNTs and CNFs can be modified by the application of different thermal treatments. In this regard, Chernyak et al. (2016) investigated the thermal stability of surface functional groups on oxygen-functionalized CNTs after different thermal treatment conditions and stages (catalyst carbonization, catalyst activation or reduction, and FTS reaction). They observed that most of the carboxylic groups decomposed in the first stage carried out at 400°C, whereas a decrease in content of all oxygen functional groups was mainly observed after the catalyst reduction stage at 400°C, specially due to the decomposition of hydroxyl and ether groups. Only the more thermally stable oxygen surface groups, such as quinones and phenols, remained stable on the support surface after 70 h of FTS reaction at 190°C, 1 bar, H<sub>2</sub>/CO of 2 and SV of 2.2 m<sup>3</sup>kg<sub>cat</sub><sup>-1</sup>h<sup>-1</sup>. The authors highlighted that these oxygen surface groups together with the CNT defects and the CNT surface geometry effects might have prevented Co from sintering during the catalytic reaction, given that the catalysts were not deactivated with time-on-stream. In contrast, nitrogen groups were significantly more stable upon heating. Thermal treatment of nitrogen-containing CNTs at 600°C only caused a minor loss of pyridine and quaternary type nitrogen groups Kundu et al. (2010).

Xing et al. (2013) compared the FTS performance of Co-based catalysts supported on oxidized and thermally treated CNTs in inert atmosphere at 450, 650, and 900°C. The results of the FTS reaction revealed that the oxidized Co/CNT catalysts treated at 650°C (Co/CNTs-650) presented the highest CO conversion (89.3%), the lowest CH<sub>4</sub> selectivity (8.4%), and the highest C<sub>5+</sub> hydrocarbon selectivity (83.7%) among all the tested catalysts (entry 12 and 13, **Supplementary Table S3**). They claimed that it was possible to partially remove the oxygen-containing functional groups from the surface of CNTs by controlling the thermal treatment temperature, while keeping the integrity of inner CNT walls and thus controlling the preferential encapsulation of cobalt

clusters (80% for Co/CNTs-650) with optimal size (5–10 nm) inside the CNTs.

The role of oxygen- and nitrogen-functionalized CNTs as supports for Fe-based FTS catalytic systems was also investigated. Malek Abbaslou et al. (2009) studied the acid treatment (35 wt% HNO<sub>3</sub>) of CNTs with different BET surface areas at 25 and 110°C. These materials were used as support for the preparation of Fe-based catalysts for FTS. The resultant Fe/CNT catalysts revealed that the more severe the acid-treatment temperature and the higher BET surface area (46 m<sup>2</sup>/g for Fe/ha-lsa-C and 200 m<sup>2</sup>/g Fe/ha-hsa-C) of the CNT-supported Fe catalysts, the higher the activity, stability, and selectivity to C<sub>5+</sub> hydrocarbons of the catalysts (entries 16 and 17, **Supplementary Table S3**).

Schulte et al. (2012) compared N-doped CNTs (N-CNTs) with conventional oxygen-functionalized CNTs as supports for iron catalyst for FTS. The supports were pretreated by gas phase NH<sub>3</sub> or HNO<sub>3</sub> vapor, respectively. They observed that doping CNTs with nitrogen enhanced Fe species dispersion and, as a result, an almost two-fold higher FT activity was found for Fe supported on the N-doped CNT (20Fe/N-CNT) as compared to the one of Fe supported on the oxidized CNT (20Fe/O-CNT) (entries 19 and 20, **Supplementary Table S3**). They suggested that high electric conductivity and good metal dispersion ability were the main advantages for the N-NCT support. These results were later supported by Chew et al. (2016).

On this context, Xiong et al. (2014a) reported a novel approach to prepare N-CNTs by a postdoping method in which acetonitrile was passed over CNTs at 700 and 900°C, and N atoms were homogeneously deposited on the CNT surface (so that the resulting N-CNTs contained 1.75 wt% N). The N-CNTs were later treated with HNO<sub>3</sub> prior to iron deposition. The resulting catalysts were tested in the HT-FTS reaction (entry 18, **Supplementary Table S3**). The surface N was in the form of pyridinic, quaternary, and pyridinic oxide type nitrogen. They observed that the Fe/N-CNT catalysts were more difficult to reduce than the corresponding Fe/CNT catalysts due to the prefunctionalization with nitrogen atoms. However, the Fe/N-CNT catalysts showed superior FTS activity when comparing with that of Fe/CNT catalysts. Therefore, N-doping seems to have a very positive effect on the FT catalyst performance, being it even superior than those results obtained for oxidized CNTs as supports of FT catalysts. In fact, as it can be observed in **Supplementary Table S3**, Fe supported on N-doped CNTs presents the highest metal-time yield (MTY) operating at HT-FTS conditions.

### Effect of Catalyst Preparation Methods

Various catalyst preparation methods to support FT catalysts on CNTs have been investigated and compared, including IWI, wetness impregnation (WI), homogeneous deposition-precipitation (HDP), colloidal synthesis technique, and most recently, a modified photo-Fenton process. Among of all of them, the standard IWI method is the most frequently used for fundamental studies. **Table 3** compares the FT catalytic performance of the most relevant unpromoted Co and Fe catalysts supported on CNTs and CNFs prepared using different catalysts preparation methods. Further details are

reported in the supporting information file (**Supplement Table S4**) as the prefunctionalization method, metal particle size, C<sub>2</sub>-C<sub>4</sub> O/P ratio and  $\alpha$  value obtained from FTS. For example, it was found that using ethanol as a solvent for cobalt impregnation on oxidized CNTs and untreated CNTs showed a superior FTS activity as compared to those prepared from an aqueous solution and propanol (entries 1–2, **Table 3**) (Bezemer et al., 2006a; Eschemann et al., 2015). Eschemann et al. (2015) emphasized that choosing ethanol as solvent and an appropriate drying procedure reduced the average cobalt cluster size on the CNT surface and improved the metal dispersion.

The comparison of Co/CNT prepared by IWI (Co/CNT-IM) and the HDP method (Co/CNT-DP), using urea as the precipitation agent, showed that the catalysts prepared by IWI were 2.6 times more active, which was attributed to lower cobalt particle size and improved metal dispersion on the latter case (entries 3 and 4, **Table 3**) (Xiong et al., 2011).

Recently, Almkhelfe et al. (2018) investigated Co and Fe catalysts prepared in a single step by a modified photo-Fenton process without the need of a prefunctionalization stage, which showed higher CO conversion, selectivity to C<sub>5+</sub> hydrocarbons, and an improved catalyst stability compared to those of the catalysts prepared *via* IWI at low FTS reaction temperatures (200 and 250°C for Co- and Fe-based catalysts, respectively, 10 bar and H<sub>2</sub>/CO of 2). The main cause of the outstanding behavior for the photo-Fenton-prepared catalysts was the higher metal dispersion and optimal catalyst particle sizes with a narrow particle size distribution. In particular, the Co/CNT catalysts prepared from the photo-Fenton approach showed a CO conversion of 80% and a selectivity for liquid hydrocarbons of 70%, which is among the highest values reported for FTS (entry 6, **Table 3**).

Ismail et al. (2019) investigated the FT catalyst performance of Co/CNT catalysts prepared by a colloidal synthesis process (cs<sub>Co100</sub>/CNT) and IWI (ci<sub>Co100</sub>/CNT). It was found that the colloidally synthesized Co catalysts showed higher catalytic activity, higher selectivity toward C<sub>2</sub>-C<sub>4</sub> fraction, and lower selectivity to C<sub>5+</sub> hydrocarbons than the Co/CNT catalysts prepared by IWI at 1 bar and 220°C (entries 7 and 8, **Table 3**). Nevertheless, colloidally synthesized cobalt catalysts were previously reported to have a very high selectivity to long hydrocarbon chain at higher reaction pressure (20 bar and 220°C), given that high-pressure conditions promote C<sub>5+</sub> product formation (Trépanier et al., 2010; Van Deelen et al., 2018).

The modification of the Co and Fe/CNT FTS catalysts by thermal treatments was also investigated. Chernyak et al. (2020) studied the effect of sintering temperature (800–1,200°C) on the structure and FTS catalytic performance of Co and Fe CNT-supported catalyst prepared by IWI *via* the spark plasma sintering approach (Co800 and Fe800, entries 9 and 17, **Table 3**). The sintered catalysts presented higher activity and selectivity to C<sub>5+</sub> liquid hydrocarbons during FTS, as compared to those nonthermally treated catalysts and without the application of a prereduction step. The main reason was the presence of carbon-encapsulated metallic nanoparticles embedded in the CNT

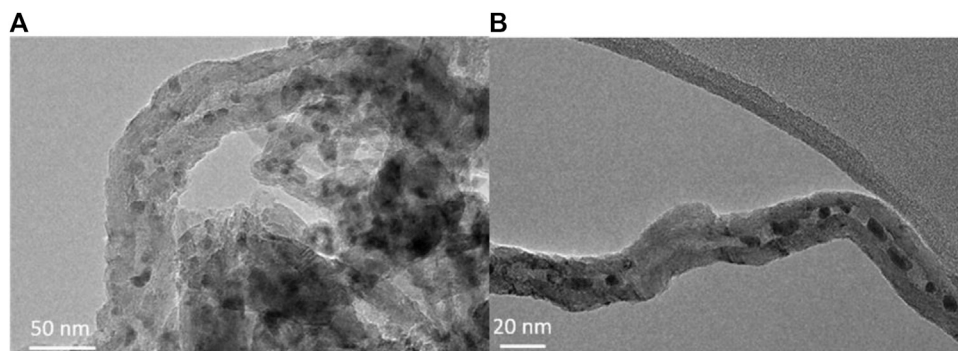


**FIGURE 6** | TEM images of the fresh confined and nonconfined Fe catalysts: **(A)** Fe/CNT-out, **(B)** Fe/CNT-in. Reprinted from Gu et al., 2019, B., He, S., Peron, D.V., Strossi Pedrollo, D.R., Moldovan, S., Ribeiro, M.C., Lobato, B., Chernavskii, P.A., Ordonsky, V.V., and Khodakov, A.Y. Synergy of nanoconfinement and promotion in the design of efficient supported iron catalysts for direct olefin synthesis from syngas. *Journal of Catalysis*, 2019, 376, 1-16, copyright 2019, with permission from Elsevier.

framework. In the case of the sintered Fe/CNT catalyst, the close contact between the metallic site and the carbon material after the sintering approach facilitated the formation of the active iron carbide phase. It should be also highlighted the calculated TOF values for Co800 ( $0.10 \text{ s}^{-1}$ ) and for Fe800 ( $\sim 1.0 \text{ s}^{-1}$ ), which were remarkably high as compared to other unpromoted FTS catalysts.

In a recent work, the controlled synthesis of cobalt catalyst with single hcp-Co supported on CNF was carried out through the controlled formation of a CoO oxide precursor, followed by a reduction step (entry 11, **Table 3**). Compared to the conventional reduction-carburization-reduction (RCR) process (entry 10, **Table 3**), this method improved Co particle dispersion and LT-FTS activity by avoiding sintering of the nanoparticles after reduction. Furthermore, this catalyst was catalytically stable for 400 h at the operation conditions studied (Lyu et al., 2019).

### Effect of Pore Size

CNT pore confinement of the FT active phase and the effect of the support pore size have also shown to influence the activity and selectivity of the catalysts for FTS. As aforementioned, the pore size of the CNTs can be associated to both the inner diameter of the tube or to aggregated pores caused by CNT interaction.

On this context, Fu et al. (2014b) studied Co/CNT catalysts prepared by IWI with different CNT outer diameters (<8, 20–30, and 30–60). It was found that larger CNT outer diameters resulted in the formation of bigger  $\text{Co}_3\text{O}_4$  crystallites and greater reducibility, but the larger sizes also resulted in less Co dispersion. The catalyst with larger outer diameters of 30–60 nm and pore sizes displayed higher TOF and selectivity to  $\text{C}_{5+}$  hydrocarbons, which was due to the suitable particle sizes and the better crystallized graphitic structure for the support with larger pore sizes, which promoted CO conversion. These results are in line with the observations by Xie et al. (2012) about the FTS performance of Co/CNT catalysts with different outer diameters. In contrast, Zhang et al. (2009) observed that the diameter of carbon nanotubes seemed to have negligible impact on the FTS performance of Co/CNT catalysts.

The effects of pore diameters of Fe catalysts supported on CNT on the FTS reaction rates and product selectivity were also

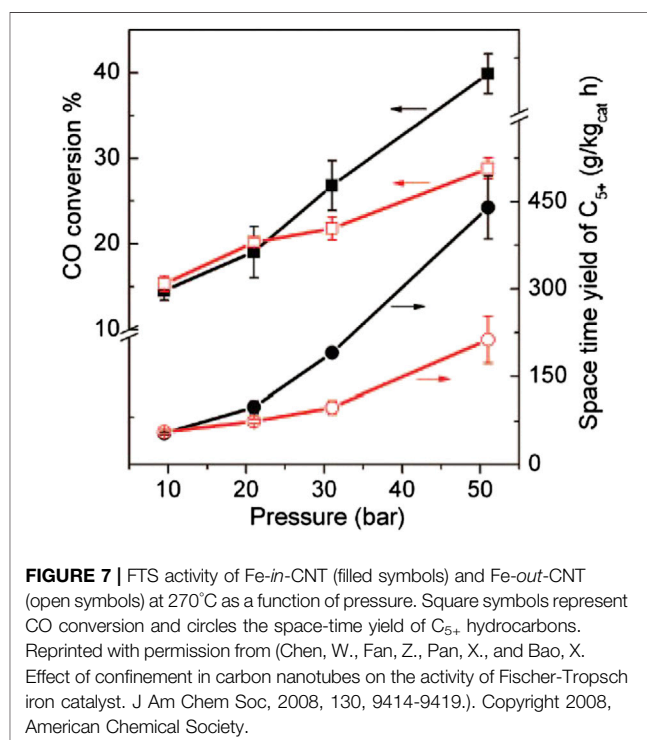


**FIGURE 7** | FTS activity of Fe-in-CNT (filled symbols) and Fe-out-CNT (open symbols) at 270°C as a function of pressure. Square symbols represent CO conversion and circles the space-time yield of  $\text{C}_{5+}$  hydrocarbons. Reprinted with permission from (Chen, W., Fan, Z., Pan, X., and Bao, X. Effect of confinement in carbon nanotubes on the activity of Fischer-Tropsch iron catalyst. *J Am Chem Soc*, 2008, 130, 9414-9419). Copyright 2008, American Chemical Society.

studied. Abbaslou et al. (2010) showed that both the selectivity to  $\text{C}_{5+}$  hydrocarbons and the CO conversion were improved for Fe/CNT catalysts with the narrower pore structure. Deposition of iron inside the nanotubes ( $\sim 80\%$  according to the TEM images) with narrower pore structure resulted in smaller metal particle size (12 nm compared to 17 nm of Fe/wp-CNT catalyst with wider pore structure) and better metal dispersion. These features conferred the catalyst a better extent of reduction and an improved catalytic performance.

### Effect of Catalyst Pore Confinement

In general, metal catalysts encapsulated inside CNTs are obtained by direct incorporation during the pyrolysis of precursor mixtures, such as ferroceneacetylene (Karmakar et al., 2004),

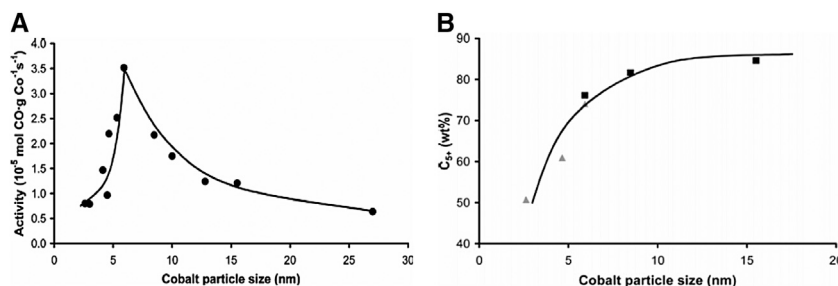


**FIGURE 8 |** The influence of cobalt particle size on **(A)** FT synthesis activity normalized to cobalt loading (220°C, H<sub>2</sub>/CO = 2, 1 bar) and **(B)** the C<sub>5+</sub> selectivity measured at 35 bar, data markers in black at 210°C and in gray at 250°C. Figure reprinted with permission from (Bezemer, G.L., Bitter, J.H., Kuipers, H.P.C.E., Oosterbeek, H., Holeyijn, J.E., Xu, X., Kapteijn, F., Van Dillen, A.J., and De Jong, K.P. Cobalt Particle Size Effects in the Fischer-Tropsch Reaction Studied with Carbon Nanofiber Supported Catalysts. *Journal of the American Chemical Society*. 2006, 128, 3956-3964). Copyright 2006, American Chemical Society.

by metal deposition on CNTs with opened tips after a strong-acid pretreatment (Chen et al., 2008) or by a two-step IWI methods, first with an aqueous solution and later with the metal precursor solution (Abbaslou et al., 2009). **Figure 6** shows TEM images of confined and nonconfined Fe catalysts.

The research group of professor Bao Xinhe (Chen et al., 2006; Chen et al., 2007; Chen et al., 2008) evidenced that iron species located inside the CNT tubes (Fe-*in*-CNT) had better reducibility and tended to form a more active iron carbide phase under reaction conditions than iron located outside the CNT channels (Fe-*out*-CNT). This caused a remarkable enhanced activity in LT-FTS and the favored formation of C<sub>5+</sub> hydrocarbons working from 20 to 50 bar at 270°C and H<sub>2</sub>/CO of 2 (entries 18–19, **Table 3**). This has been recently supported by Gu et al. (2019). **Figure 7** shows the catalytic performance of the Fe-*in*-CNT and Fe-*out*-CNT catalysts during FTS as a function of the pressure reported by Chen et al. (2008). This behavior was attributed to the modified redox properties of the confined iron catalysts and to the trapping effect of the reaction intermediates inside the CNTs, which was suggested to increase their contact time with iron catalysts, favoring the growth of longer chain hydrocarbons.

Several authors also investigated the confinement effect of cobalt particles inside CNT on the FTS catalyst performance. Tavasoli et al. (2010) confirmed that encapsulation of the Co catalytic sites inside the CNTs resulted in lower rates of sintering of the Co nanoparticles as compared with the particles located on the outer layer of the CNTs. Furthermore, Xie et al. (2012) and Fu et al. (2014b) agreed that the FTS activity and the selectivity to C<sub>5+</sub> hydrocarbons was improved over the catalysts with most of the Co nanoparticles located inside the CNT due to the enhanced catalyst reducibility and to the favorable chain growth of the intermediates formed inside the tubes.

### Effect of Metal Particle Size

Professor De Jong and co-workers reported the influence of both metallic cobalt and iron carbide particle size of graphitic CNFs (Co/CNFs and Fe/CNFs) as support for the FTS reaction under 1 and 35 bar (Bezemer et al., 2006a; Torres Galvis et al., 2012a). In this regard, Bezemer et al. (2006a) found that the

surface-specific activity (apparent TOF) in the FT reaction was independent of cobalt particle size for unpromoted cobalt catalysts with sizes larger than 6 nm at 1 bar or 8 nm at 35 bar (220°C, H<sub>2</sub>/CO = 2) [11]. The authors attributed the lower TOF values of the catalysts with Co particles smaller than 6 nm as the result of a significant increase in the CH<sub>x</sub> intermediates residence time combined with a decrease of the CH<sub>x</sub> coverage and, among others, to the presence of irreversible bonded CO molecules on smaller particles, which causes partial blockage of the Co surface (Den Breejen et al., 2009). These results have been later supported for Co/AC, Co/CNT, Co/CNF, Co/CSs, and Co-MOFMS catalysts (Xiong et al., 2011; Fu et al., 2014b; Luo et al., 2019).

On the other hand, both the activity and the selectivity of the CNF-supported cobalt catalysts were strongly influenced by the catalysts with smaller cobalt particle sizes. **Figure 8** shows the CoTY (**Figure 8A**) and the selectivity to C<sub>5+</sub> hydrocarbons (**Figure 8B**) for Co supported on CNF as a function of the cobalt particle size at 35 bar (Bezemer et al., 2006a). It was found a volcano-like curve for the CoTY as a function of the cobalt particle size with a maximum CoTY at 5–6 nm. Furthermore, the selectivity to C<sub>5+</sub> hydrocarbons increased with the cobalt particle size up to 15 nm, whereas the opposite trend was observed for the production of methane. The higher selectivity to methane of small Co particles was mainly attributed to their higher hydrogen coverage. A similar result for a Co/CNF catalyst was reported by Den Breejen et al. (2010). They agreed that the increase of the cobalt particle size positively affected the selectivity to C<sub>5+</sub> hydrocarbons, especially for particle sizes lower than 8 nm. In addition, the selectivity to C<sub>5+</sub> was constant for Co particle size from 8 to 15 nm. A similar positive relationship between cobalt particle size (<45 nm in diameter) and C<sub>5+</sub> selectivity on Co/CNTs, Co/carbon-sphere, and Co-derived MOF catalysts was also reported (Xiong et al., 2011; Luo et al., 2019).

Torres Galvis et al. (2012a) investigated the influence of the Fe carbide particle size of CNF-supported catalysts. The TOF based on the initial activity of unpromoted catalysts increases 6–8 times at 1 bar (350°C, H<sub>2</sub>/CO = 1) when the average iron carbide particle size decreased from 7 to 2 nm, whereas the selectivity

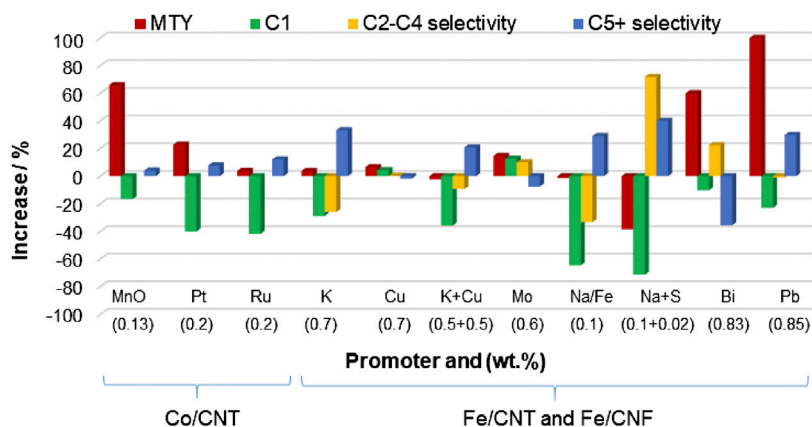


**FIGURE 9** | Increase in metal-time yield and C<sub>1</sub>, C<sub>2</sub>-C<sub>4</sub>, and in selectivity to C<sub>5+</sub> hydrocarbons for different promoted Co- and Fe-supported catalysts on CNFs and CNTs compared to those of the unpromoted counterpart. The title in the x-axis indicates the promoter and its concentration in wt%. Data are adapted from refs. (Bahome et al., 2005; Bezemer et al., 2006b; Malek Abbaslou et al., 2011; Zhang et al., 2011; Cheng et al., 2015; Xie et al., 2016; Gu et al., 2018). Reaction conditions: MnO-, Pt-, or RuCo/CNT (H<sub>2</sub>/CO = 2, 220°C, 20 bar), K- and/or Cu-Fe/CNT (H<sub>2</sub>/CO = 2, 275°C, 8 bar), Mo-Fe/CNT (H<sub>2</sub>/CO = 1, 275°C, 20 bar), Na-Fe/CNT (H<sub>2</sub>/CO = 2, 300°C, 20 bar), Na and S-Fe/CNT (H<sub>2</sub>/CO = 1, 340°C, 20 bar), and Bi- or Pb-Fe/CNF (H<sub>2</sub>/CO = 1, 350°C, 10 bar).

to methane and lower olefins remained constant. On the other hand, Ru nanoparticles supported on CNTs, AC, and graphite have been also studied. Kang et al. (2009) reported that Ru nanoparticles supported on carbon nanotubes with a mean particle size of 7 nm, exhibited the highest selectivity toward C<sub>10</sub>-C<sub>20</sub> (60%) and TOF for CO conversion at 260°C, 20 bar and H<sub>2</sub>/CO = 1.

### Cobalt and Iron Bimetallic Catalysts and Effect of Promoters on Fischer-Tropsch Synthesis

The combination of cobalt and iron in a bimetallic-supported catalyst has been investigated in the last years. This interest stems from the prediction that the simultaneous use of CoFe bimetallic catalysts will give rise to a “synergistic” effect between the two active phases on the FT process. However, the studies reported on these bimetallic catalytic systems are a bit contradictory. In addition to this, optimization of Co-, Fe-, and CoFe-supported CNT and CNF catalysts for FTS process, especially related to product selectivity, can be addressed by catalyst promotion. Among various promoters, MnO and noble metals such as Pt and Ru have been incorporated to cobalt-supported CNF and CNT catalysts, whereas K, Cu, Mo, Na, S, Bi, and Pb have been added to Fe/CNFs and Fe/CNTs catalysts. **Figure 9** represents the increase in CO conversion and selectivity to C<sub>2</sub>-C<sub>4</sub> and C<sub>5+</sub> products for different promoted Co and Fe catalysts supported on CNFs and CNTs compared to those of the unpromoted counterpart, whereas **Supplementary Table S5** summarizes the FTS performance of bimetallic and promoted cobalt and iron catalysts supported on CNTs and CNFs.

Tavasoli et al. (2009) conducted some studies on CoFe/CNT catalysts and found that cobalt catalyst with 0.5 wt% of Fe increased the CO conversion with minor modifications of the selectivity to C<sub>5+</sub> hydrocarbons during LT-FTS (entry 1, **Supplementary Table S5**). However, incorporation of 4 wt%

of iron to the bimetallic catalyst resulted in a decrease of the catalyst activity and selectivity to C<sub>5+</sub> hydrocarbon, whereas the alcohol selectivity notably increased. This behavior was attributed to the formation of Co-Fe alloys. Contrary to this, another study found that cobalt and iron supported on CNFs with a metal loading of 10 wt% Co and 5 wt% Fe (10Co5Fe/CNF), tested at 250°C and H<sub>2</sub>/CO of 2, presented the highest yield to long-chain hydrocarbons, with minor selectivity to methane and carbon dioxide (Díaz et al., 2014). These studies agreed that the incorporation of iron to cobalt catalysts improved the dispersion of cobalt on the support and facilitated the reduction of iron species to the metallic form. In a recent study, Ismail et al. (2019) found that colloiddally synthesized bimetallic Co<sub>50</sub>Fe<sub>50</sub>/CNT catalyst had considerably higher FT activity than the monometallic iron catalyst prepared by the same method and similar to the monometallic cobalt one under atmospheric pressure, 220°C and H<sub>2</sub>/CO of 2. Furthermore, a significant selectivity to C<sub>5+</sub> hydrocarbon and lower selectivity to CH<sub>4</sub> were obtained for the bimetallic catalyst. The authors attributed this behavior to the role of iron enhancing the distribution of cobalt species over the carbon support, in line with the aforementioned studies, and to the presence of Co-Fe alloys.

Several authors have investigated the incorporation of Pt and Ru promoters to the Co/CNT catalytic system and tested their performance in LT-FTS. Promotion with 0.2 wt% of Pt or Ru resulted in a significantly enhanced cobalt catalyst reduction and slight increase in the CoTY and C<sub>5+</sub> hydrocarbon selectivity (82.5% for RuCo/CNTs and 79.2 for PtCo/CNTs) with respect to the unpromoted catalysts, **Figure 9** and entries 5 and 6 in **Supplementary Table S5** (Zhang et al., 2011). Similar conclusions were obtained by Trépanier et al. (2009a) for the 0.5 wt% Ru-promoted Co/CNT catalyst and significant C<sub>5+</sub> hydrocarbon selectivity of 77% was also obtained (entry 7, **Supplementary Table S5**). Recently, the comparison of

Co-Ru/CNT catalyst (4 wt% Ru) prepared by the chemical reduction method and IWI showed that the Co-Ru/CNT catalysts synthesized by the reduction technique (entry 8, **Supplementary Table S5**) increased the FTS rate by 11% and the C<sub>5+</sub> selectivity by 16% when compared to that obtained through the impregnation method. Moreover, these Ru-promoted catalysts outperform the unpromoted catalyst. The different in the performance of the catalysts was attributed to the different crystallite sizes and the catalyst reduction enhancement for the Ru-promoted catalysts (Shariati et al., 2019).

The research group of professor De Jong investigated the influence of MnO on Co/CNT catalysts under LT-FTS conditions (Bezemer et al., 2005; Bezemer et al., 2006b). MnO was reported to favorably affect both activity and selectivity to C<sub>5+</sub> hydrocarbons, depending on concentration and reaction conditions. They concluded that the CoTY increased c.a. 65% and the C<sub>5+</sub> selectivity increased c.a. 4% with respect to the unpromoted catalyst after incorporation of 0.13 wt% MnO (**Figure 9**). The promoter effect was suggested to originate from a lower degree of cobalt reduction and moderation of hydrogenation reactions. On this research line, Liu and Li (2020), based on a computational study, have recently proposed a promising and novel Co/Mn bimetallic center supported on N-doped CNTs as an efficient FTS catalytic system for the production of long-chain hydrocarbons.

0.7 wt% K-promoted Fe/CNT catalysts decreased the catalyst reducibility, decreased FT rate, increased the yield of CO<sub>2</sub> and C<sub>2</sub> olefins, and reduced the methane selectivity, when compared with unpromoted catalysts (Bahome et al., 2005; Trépanier et al., 2009a). However, promotion with 0.7 wt% Cu did not greatly influence the FT product selectivity (**Figure 9** and entries 10–11, **Supplementary Table S5**). In other work, a synthesized K-doped MnO<sub>2</sub>-coated CNT composite was used to support iron catalysts (7.9 wt% Fe, 15.7 wt% Mn, and 1.9 wt% K) (Wang et al., 2015). It was found a remarkable selectivity to C<sub>2</sub>-C<sub>4</sub> olefins (50.3%) and higher CO conversion than FeMnK/CNT catalyst prepared by the coimpregnation method using CNTs as support. This was associated to the small-sized and narrow nanoparticle distribution, high dispersion of the promoters, and the weak metal-support interaction.

Combined promotion of Fe/CNF catalysts with 0.1 wt% Na and 0.2 wt% S was shown to improve the selectivity to light olefins at low conversions operating at HT-FTS conditions (**Figure 9** and entry 15, **Supplementary Table S5**) (Xie et al., 2016). The comparison with the unpromoted Fe/CNF revealed a notable enhanced iron carburization and higher initial catalytic activities over the promoted iron catalysts with Na and S.

More recently, professor Khodakov and collaborators (Gu et al., 2018; Gu et al., 2019) found extremely strong promotion effect of Bi and Pb on the catalytic performance of Fe/CNT catalysts. Compared to the unpromoted catalysts, a significant increase in FT reaction rate and a higher selectivity to the C<sub>2</sub>-C<sub>4</sub> olefins (55–60%) at 10 bar were obtained (**Figure 9** and entries 16 and 17, **Supplementary Table S5**). The promoting effects of Bi and Pb on iron catalysts have been reinforced by their preferential localization at the surface of iron carbide nanoparticles leading to the formation of core-shell structures. Furthermore, the presence

of Bi enhanced the catalyst reducibility and facilitated carburization of iron nanoparticles. For example, the FeTY was  $82 \times 10^{-5} \text{ mol}_{\text{CO}} \text{ g}_{\text{Fe}}^{-1} \text{ s}^{-1}$  for the FePb/CNT-*in* catalyst at 350°C, total syngas pressure of 10 bar, and SV of  $17 \text{ m}^3 \text{ kg}^{-1} \text{ h}^{-1}$ , which is one of the best results for unpromoted and promoted iron-based FTS catalysts available so far in the literature.

To sum up, from **Figure 8**, it can be concluded that promotion with MnO to Co/CNTs catalysts produced a very significant increase of CoTY with respect to the unpromoted catalyst, whereas promotion of Bi and Pb enhanced considerably the FeTY in Fe/CNT catalysts. Regarding the selectivity values, it should be remarked that promotion with K+Cu and Na enhanced selectively C<sub>5+</sub> formation over Fe/CNT catalytic systems with respect to the unpromoted catalysts compared under very similar FeTY values.

## Catalysts Supported on Carbon Spheres

Since the discovery of buckminsterfullerenes, spherically shaped carbons or carbon spheres (CSs) are receiving great attention from the scientific community (Ugarte, 1992). The preparation of CSs is usually accomplished by two major approaches. On the one hand, the chemical vapor deposition (CVD) method involves high-temperature decomposition of a carbon-based material under inert atmosphere, typically in the absence of a catalyst (Serp et al., 2001). This noncatalytic synthesis procedure allows the direct preparation of CSs with low surface areas (<10 m<sup>2</sup>/g) and high purity (Xiong et al., 2011; Yang et al., 2014). The surface of these CSs prepared by CVD is composed of graphitic layers/flakes with sizes ranging from 1 to 10 nm (Xiong et al., 2011), which can be arranged in different structures, forming concentric, radial, or random configurations (Serp et al., 2001). They are reported to be good model catalyst supports in FTS (Xiong et al., 2010). On the other hand, hydrothermal carbonization (HTC) process, where a carbon source (i.e., sucrose, glucose, and resorcinol) is hydrothermally treated between 80 and 250°C in an autoclave reactor, has been also proposed for the preparation of these shaped carbons (Hu et al., 2010). Compared to other preparation routes, the HTC process has some advantages, including low toxicological impact of materials and processes, easy instrumentation and techniques, the use of renewable sources, and a high energy and atom economy. Carbon spheres prepared by the HTC approach are characterized by a hydrophobic core and a hydrophilic shell with abundant surface OH and C=O groups. These CSs usually have intrinsic porous structures with controllable morphology and surface functionality. Furthermore, coupling either hard- or soft-templating effect with the HTC process has shown interesting results in the preparation of hollow carbon spheres (HCSs). The textural parameter range of typical Fe- and Co-supported CSs used in the FTS reaction are shown in **Table 1**. The BET surface area for the Fe- and Co-supported CSs prepared *via* the HTC approach can vary between 143 and 465 m<sup>2</sup>/g, whereas the total pore volume can vary between 0.2 and 0.59 cm<sup>3</sup>/g (Cheng et al., 2019; Phaahlamohlaka et al., 2020). **Supplementary Table S6** summarizes the FTS performance of Fe- and Co-supported CS catalysts.

The effect of support pretreatment, catalyst preparation methods, and promoters on the FTS performance of Fe- and

Co-supported CSs have been investigated. In the case that hollow carbon spheres (HCSs) were used as supports, the effect of catalyst confinement was studied.

### Effect of Support Functionalization and FT Catalyst Preparation Methods

CSs prepared by the CVD process are characterized for exhibiting a high carbon purity and an inert surface chemistry. In order to achieve a high metal dispersion when using these carbon materials as catalyst supports, CSs have to be functionalized with different oxygen and/or nitrogen surface groups. On the contrary, CSs obtained by the HTC approach usually do not require functionalization due to their hydrophilic shell with abundant oxygen functional groups.

Yu et al. (2010) were pioneers in reporting the use of iron-containing CSs in the FTS process. The authors reported a one-stage route for the preparation of  $\text{Fe}_x\text{O}_y/\text{C}$  spheres embedded with highly dispersed iron oxide nanoparticles by the hydrothermal treatment of a glucose solution mixed with iron nitrate under mild conditions. A steady-state CO conversion of 76% and a selectivity to  $\text{C}_{5+}$  hydrocarbons of 60% were obtained. In particular, the selectivity values to  $\text{C}_{5+}$  hydrocarbons are even better than the values reported for unpromoted iron catalysts, including Fe-*in*-CNT and Fe-*out*-CNT catalysts tested under similar FTS conditions (at 270°C, 20 bar and  $\text{H}_2/\text{CO}$  of 1) (Table 3). The remarkable catalytic activity and stability was associated to the favorable formation of iron carbides during  $\text{H}_2$  activation, which were embedded into the carbonaceous matrix.

Professor Coville and collaborators (Xiong et al., 2010; Xiong et al., 2011) carried out a comprehensive study on the prefunctionalization treatments (with  $\text{HNO}_3$  or  $\text{KMnO}_4$ ) and preparation catalyst methods (IWI and HDP) of CS-supported Fe and Co catalysts. The higher the  $\text{HNO}_3$  treatment temperature (up to 90°C), the higher degree of functionalization and metal dispersion achieved in the final catalysts. They observed that in both cases, for Fe- and Co-supported CSs, the catalysts prepared using iron/cobalt nitrate and the HDP method using urea as precipitation agent (Fe/CSs-C-DP and Co/CS-C-DP) showed the highest MTY for the FTS reaction among the different catalysts prepared, which was attributed to the smallest average metal particle size and highest metal dispersion (entries 2 and 13, Supplementary Table S6). Functionalization using nitric acid or  $\text{KMnO}_4$  showed comparable catalytic activity and  $\text{C}_{5+}$  hydrocarbon selectivity.

More recently, Kuang et al. (2019) prepared Co/CS catalysts by thermal decomposition (TD), IWI, and ultrasonic impregnation (UI) methods. The preparation of the CS support was carried out by the hydrothermal approach using an aqueous glucose solution followed by carbonization at 800°C in  $\text{N}_2$ . The catalyst prepared by the TD method (CoO/C-TD) presented the highest metal dispersion and, as consequence, remarkably higher CO conversion (21%) and selectivity to  $\text{C}_{5+}$  hydrocarbons (81.9%) during LT-FTS.

Regarding the use of N-doped CSs as supports, Xiong et al. (2014b) investigated Fe-supported N-doped CS catalysts for HT-FTS prepared by different strategies. It was suggested that the presence of pyrrolic and pyridinic N atoms is essential in

anchoring and stabilizing Fe atoms to the carbon surface, whereas quaternary N atoms play a minor role. Among all of them, the Fe-supported N-doped CSs *via* CVD of a mixture of acetylene and  $\text{CH}_3\text{CN}$  in a vertical furnace (Fe/NCS<sub>ver</sub>) had the highest N content (4 wt%, mainly pyrrolic and pyridinic N atoms) and well-dispersed Fe oxide particles on the N-doped CSs. Therefore, Fe/NCS<sub>ve</sub> catalyst exhibited the highest FT activity and selectivity to  $\text{C}_{5+}$  hydrocarbons (entry 3, Supplementary Table S6).

More recently, Cheng et al. (2019) studied the preparation of N-doped CSs using biomolecule dopamine as carbon and nitrogen sources and they are used as supports for cobalt catalyst. In line with the observations reported by Xiong et al. (2014b), the sample with the highest content of pyrrolic N and smallest cobalt particle size (that pretreated at 500°C, Co/NCS-500) exhibited the highest CO conversion and  $\text{C}_{5+}$  hydrocarbon selectivity under LT-FTS reaction (entries 14 and 15, Supplementary Table S6).

### Cobalt and Iron Bimetallic Catalysts and Effect of Promoters

Dlamini et al. (2015) prepared a series of Fe-Co bimetallic-supported CS catalysts and investigated their use in the FTS reaction. The addition of small amounts of Fe to Co-based catalyst resulted in an enhancement of the CO conversion, being its maximum for the catalyst containing 0.5 wt% Fe and 9.5 wt% Co (entry 17, Supplementary Table S6). Fe/Co alloy formation was detected upon reduction above 450°C, but its relative amount was not correlated with higher  $\text{C}_{5+}$  selectivity. The bimetallic catalysts with iron content higher than 2 wt% showed the highest  $\text{C}_{5+}$  selectivity (87%) at a CO conversion of 21%.

Zhang et al. (2015) carried out a deep study on the effect of different promoters (Na, K, Mn, and Zn) over Fe-supported CSs prepared through one pot solvothermal method and their use in the FTS process. The catalytic experiments showed that K, Na, and Zn promotion resulted in an enhancement of the CO conversion values as compared to that of the unpromoted catalyst. However, Mn promotion resulted in the decrease of the CO conversion. The FTS results revealed that Na was the one enhancing the catalytic performance to the most. Na promotion strongly decreased the methane generation, producing more  $\text{C}_{5+}$  hydrocarbons and enhancing the O/P ratio.

In this line, K- and Mn-promoted Fe-supported spherical mesoporous carbons (Fe/SMCs) were reported by Chen et al. (2018). These authors prepared spherical mesoporous carbons by a  $\text{SiO}_2$  template assisted sol-gel procedure in water-in-oil emulsions, using resorcinol and formaldehyde as carbon sources. High iron loadings were achieved (30–50 wt%), and the BET surface area was very high (397  $\text{m}^2/\text{g}$  for an iron loading of 40 wt%). 2.5 wt% K promotion decreased the FeTY and TOF values, whereas the presence of 5 wt% of Mn enhanced them.  $\text{CO}_2$  generation was diminished by the presence of Mn but enhanced by K.

The favorable effect of alkali (Na, Li, and K) promotion over iron-based CS catalysts for the HT-FTS reaction was reported by Ma et al. (2020). In this study, the promoted iron-containing CSs were prepared through a one-step hydrothermal synthesis. The

reaction results showed an improvement in the CO conversions and in the O/P ratios for all the promoted catalysts compared to the unpromoted one. Here, Na was the promoter enhancing the CO conversion value to the most, which is in agreement to the work reported by Zhang et al. (2015). The presence of the metal promoters increased the selectivity to C<sub>5+</sub> hydrocarbons following the order: Na > K > Li. A further study on the effect of Na content revealed that the CO conversion value was maximum for a Na load of 1 wt%, whereas the highest selectivity to C<sub>5+</sub> hydrocarbons was achieved for the catalyst with 2 wt% of Na.

To sum up, alkali metals result in the enhancement of the CO conversion, the olefin/paraffin ratio, and the C<sub>5+</sub> selectivity values when they are used as promoters in Fe/CS catalysts. However, in the case of cobalt-based catalysts, K promotion resulted in the decrease of the catalytic activity. On the other hand, Mn has been shown as a useful promoter for olefin generation purposes in Fe-supported CS catalysts.

### Hollow Carbon Spheres as Catalyst Supports

CNTs as support for FT catalysts have the advantage of allocating the catalytic active phase either inside or outside the nanotube. This phenomenology was also studied with HCSs. HCSs used as supports for FTS catalysts were prepared by coating a carbon precursor onto either SiO<sub>2</sub> (Phaahlamohlaka et al., 2017; Teng et al., 2018) or polystyrene (Phaahlamohlaka et al., 2020) spheres as hard and soft templates, respectively, followed by a pyrolysis stage and removal of the template. The SiO<sub>2</sub> template spheres were removed by NaOH or HF treatments, whereas polystyrene was easily removed by heat treatment under an inert environment.

For example, Phaahlamohlaka et al. (2017) and Phaahlamohlaka et al. (2020) prepared Co-supported mesoporous hollow carbon spheres (MHCSs) promoted with ruthenium and both Co and Ru nanoparticles where located either outside or inside the MHCSs. The promoted catalysts exhibited higher FTS activity compared to the unpromoted counterparts, which was attributed to a hydrogen spillover effect from Ru to Co that enhanced cobalt oxide reducibility. When Co and Ru nanoparticles were located inside the MHCSs (CoRu@HCS), higher selectivity to methane and lower selectivity to C<sub>5+</sub> hydrocarbons were obtained (entry 17, **Supplementary Table S6**). The authors attributed these differences to the confinement effect of the Co and Ru nanoparticles inside the hollow carbon structure, which gave rise to a hydrogen richer environment, which favored methane formation.

In other work, Teng et al. (2018) reported a highly efficient Fe-contained hollow CS catalyst with highly dispersed Fe<sub>2</sub>C sites embedded within the carbon matrix and successfully tested it in the HT-FTS reaction. SiO<sub>2</sub> spheres were used as hard templates with different diameter sizes (150 and 260 nm) and resorcinol and formaldehyde as carbon sources. Iron loading was carried out prior to the pyrolysis of the polymer at different temperatures (500, 600, and 700°C) under N<sub>2</sub> flow, followed by etching the template. Lower carbon thickness and higher iron particle size was evidenced from TEM when increasing the pyrolysis temperature. It was found that the catalyst calcinated at 600°C

exhibited the highest selectivity to lower olefins (30.1% in a CO<sub>2</sub>-free basis) and the highest O/P ratio (4.8). Additionally, they found a higher methane formation and lower O/P ratio when using the larger template, which was also associated to the H<sub>2</sub> enrichment effect taking place inside the hollow structure of the catalyst, being it higher when increasing the cavity size of the CS catalyst.

### Catalysts Supported on Graphene, Graphite, and Diamond

Graphene is formed by one or several layers (3 to <10) of sp<sup>2</sup>-hybridized carbon films forming a two-dimensional (2D) crystal, which is considered as the basic building block for carbon materials of different dimensionalities, such as fullerenes (0D), nanotubes and nanofibers (1D), or graphite (3D) (Geim and Novoselov, 2007). Graphite consists of van der Waals coupled graphene layers, which can be stacked slightly differently and either alpha (hexagonal) or beta (rhombohedral) graphite forms can be formed (Lipson and Stokes, 1942). On the other hand, diamond is a crystalline carbon material formed by sp<sup>3</sup> hybridized carbon atoms. **Figure 10** shows a schematic crystal structure of graphene, graphite, and diamond and (**Supplementary Table S7**) the FTS performance of FT catalysts supported on these carbon materials.

To the best of our knowledge, there is only one work of Co-loaded powdered oxidized diamond catalyst tested in the FTS reaction (Honsho et al., 2012). The authors used a commercial powdered diamond having a surface area of 24 m<sup>2</sup>/g, which was oxidized in air prior to cobalt deposition by IWI. The catalysts showed a high CO conversion of 44.5% and selectivity to C<sub>5+</sub> hydrocarbons of 62.7%. This CO conversion was significantly higher than those obtained for Co-loaded on SiO<sub>2</sub> (38.4%), AC (12.2%), and powdered oxidized graphite catalysts (2.8%) with higher surface areas. The weaker interaction between the O-DIA surface and cobalt oxide contributed to the better FTS results.

Regarding the use of graphene as supports for FTS catalysts, Moussa et al. (2014) investigated the chemical reduction of graphene oxide in water in the presence of nitrates of iron and potassium under microwave irradiation resulting in Fe<sub>15</sub>K<sub>5</sub>-G catalyst (15 wt% of Fe and 5 wt% of K). It should be highlighted that graphene oxide does not require a prefunctionalization of the support due to the presence of epoxy groups on the surface, which act as anchoring sites for the metal catalysts. The FTS catalyst was tested under HT-FTS and compared with K-promoted Fe/CNT catalyst. It was observed that the graphene oxide-supported catalyst exhibited an excellent stability, recyclability, the highest CO conversion (73.5%), and selectivity to C<sub>8+</sub> hydrocarbons (86.7%). The authors attributed the good FTS performance of the Fe<sub>15</sub>K<sub>5</sub>-G catalyst to the presence or defects within the graphene lattice, which acted as favorable nucleation sites to anchor the metal nanoparticles.

Karimi et al. (2015a) and Karimi et al. (2015b) performed a comparative study of 15Co/graphene (602 m<sup>2</sup>/g) and 15Co/CNT (372 m<sup>2</sup>/g) catalysts for the FTS reaction. Prior to catalyst preparation by IWI, both supports were treated

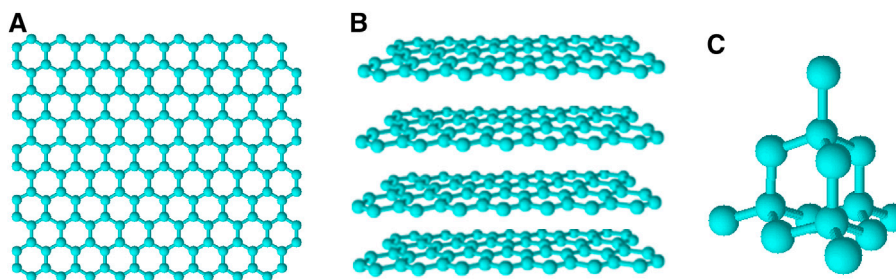


**FIGURE 10** | Crystal structure of (A) graphene, (B) graphite, and (C) diamond crystal unit.

with  $\text{HNO}_3$ . The FTS rate and CO conversion percentage obtained by 15Co/graphene were significantly larger than that obtained using 15Co/CNT catalyst. The selectivity to  $\text{C}_{5+}$  hydrocarbons was also higher for 15Co/graphene (87.1%) than for 15Co/CNTs (83.9%) at isoconversion conditions (around 60% of CO conversion). In addition, the CO conversion dropped only by 22% over 15Co/graphene after 480 h, whereas it dropped by 34% for the 15Co/CNT catalyst, which was caused in both cases by cobalt sintering. Therefore, in this study, Co-supported graphene outperformed to Co-supported CNTs catalyst under the preparation and reaction conditions used.

In this line, Hajjar et al. (2017) compared the FTS performance of cobalt catalysts supported on graphene oxide and nanoporous graphene with BET surface areas of 290 and 700  $\text{m}^2/\text{g}$ , respectively. The nanoporous graphene material was first oxidized in a mixture of sulfuric and nitric acids. As aforementioned, graphene oxide did not require functionalization. The resulting catalysts (15Co/GO and 15Co/NPG) were evaluated in the FTS reaction. The carbon nanostructured graphene-based catalysts exhibited higher CO conversion of around 65% and lower deactivation rate compared to 15Co/GO. Moreover, the selectivity to  $\text{C}_{5+}$  hydrocarbon was also significantly higher when using Co/NPG (87.4%), which was evident from the higher surface area and pore volume.

More recently, Chernyak et al. (2019) reported oxidized and N-doped graphene nanoflakes (GNFs) as supports for Co-based FT catalysts. In this work, pristine and N-doped GNFs were prepared by pyrolysis of hexane and acetonitrile, respectively. The oxidized derivatives were obtained after an  $\text{HNO}_3$  treatment, and the Co-supported catalysts were prepared by the WI method, resulting in Co-supported GNFOx (Co/GNFOx) and Co-supported N-doped GNFOx (Co/N-GNFOx) having BET surface areas of 250 and 415  $\text{m}^2/\text{g}$ , respectively. The introduction of acetonitrile at the pyrolysis stage led to the formation of predominantly bulk-distributed pyridine and graphitic nitrogen species, and the nitric acid oxidation of this material introduced the pyridone/pyrrolidone groups on the surface of the support. The catalysts were tested in the FTS reaction (entries 5 and 6, **Supplementary Table S7**). Interestingly, greatly higher TOF and selectivity to short-chain hydrocarbons ( $\text{C}_2\text{-C}_4$ ) were obtained for Co/N-GNFOx, whereas higher CO conversion and  $\text{CH}_4$  selectivity was obtained for Co/GNFOx. The presence of smaller cobalt oxide crystallites found in

Co/N-GNFOx and the higher resistance to particle sintering during catalyst activation could explain these results. However, their  $\text{C}_{5+}$  selectivity values were quite low (20–43%) due to the presence of very narrow pores on these samples (less than 1 nm), which hindered CO diffusion and increased  $\text{H}_2$  intrapore concentration.

On the other hand, a high surface area graphite material (399  $\text{m}^2/\text{g}$ ) has been used as support of cesium-promoted Ru catalysts and tested for FT reaction (entries 8 and 9, **Supplementary Table S7**). In this work, Eslava et al. (2018) claimed that the presence of  $\text{Cs}_2\text{O}$  in the catalysts prepared with  $\text{CSNO}_3$  as promoter precursor was responsible of a high selectivity to  $\text{CO}_2$  during reaction, whereas the WGS reaction, and hence the  $\text{CO}_2$  selectively, significantly decreased using  $\text{CsCl}$ .

## ANALYZING THE EFFECT OF CARBON SUPPORT STRUCTURE ON FISCHER-TROPSCH SYNTHESIS CATALYST PERFORMANCE

It has been observed that the reducibility of Co- and Fe-based catalysts is improved on carbon-based supports compared to that of oxide materials. However, the preparation of highly dispersed and stable catalysts still requires at least of intermediate interactions between the carbon support surface and the metal precursor. Modification of surface chemical properties of inert (or highly ordered) carbon-based materials, especially those prepared at high carbonization temperatures and/or from CVD of a carbon precursor, such as of CNTs, CNFs, CSs, graphite, and graphene, by introduction of oxygen and nitrogen functional groups, was found to be essential to increase their ability to stably anchor the active metal species for the FTS. Consequently, an additional prefunctionalization step prior to the catalyst preparation resulted in an increase of metal dispersion and stability on the carbon surface, positively affecting the activity of the catalyst in this reaction. On the other hand, amorphous carbons such as ACs, OMCs, and CSs, which are usually prepared at lower carbonization temperatures (especially those obtained by the HTC approach), are characterized by the presence of abundant surface oxygen functional groups. These oxygen surface groups are mainly originated from the biomass source (biomass residues in the case of ACs or isolated carbohydrates in the case of OMCs and CSs) used as carbon precursor. Therefore,

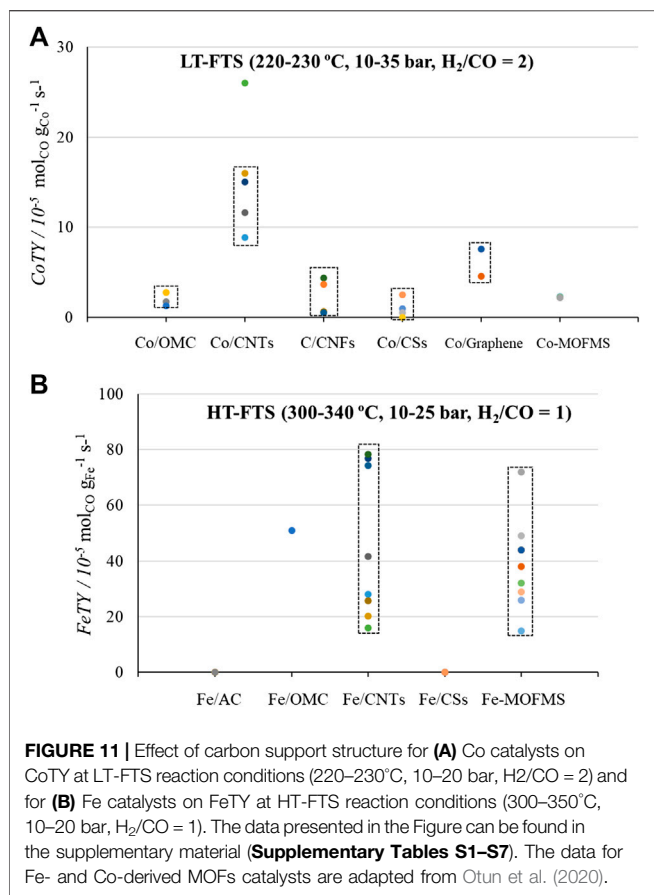


**FIGURE 11** | Effect of carbon support structure for (A) Co catalysts on CoTY at LT-FTS reaction conditions (220–230°C, 10–20 bar, H<sub>2</sub>/CO = 2) and for (B) Fe catalysts on FeTY at HT-FTS reaction conditions (300–350°C, 10–20 bar, H<sub>2</sub>/CO = 1). The data presented in the Figure can be found in the supplementary material (Supplementary Tables S1–S7). The data for Fe- and Co-derived MOFs catalysts are adapted from Otun et al. (2020).

these carbon supports did not require of a carbon surface functionalization stage. Furthermore, the use of activation agents and porous inorganic templates in the preparation of ACs and OMCs, respectively, together with the lower carbonization temperatures mostly used in the preparation of these carbon materials produced carbon supports with high BET surface areas, pore volumes, and oxygen surface groups, as shown for Co- and Fe-supported AC and OMC catalysts in Table 1. Undoubtedly, the metal loading and catalyst preparation procedure also influenced the textural characteristics and surface chemistry of the resultant catalysts, blocking part of support porosity and creating specific oxygen surface groups.

To compare the effect of carbon support structure of Co- and Fe-based catalysts on their activity for the FTS reaction, the weight specific activity (cobalt- and iron-time yield, CoTY and FeTY, respectively) and surface-specific activity (turnover frequency, TOF) were plotted for each type of carbon-based supported catalyst under similar reaction condition range, and the results are shown in Figure 11 and Supplementary Figure S1, respectively.

Clearly, a strong dependence of the FTS catalytic activity on carbon-based support structure has been observed. It is noteworthy that both the CoTY and TOF are similar for Co-based catalysts. However, the lack of TOF values (or data to be able to calculate these values) reported for Fe-based catalysts does not make comparison between these two activity indicators possible.

In general, the highest CoTY values are obtained for Co-supported CNTs, followed by Co/graphene and Co/CNFs (Figure 11A). The better crystallized graphitic structure in CNTs, which facilitate the electron transfer between the cobalt metal and CO molecules and highly stable cobalt nanoparticles, mainly dispersed inside the tubes, has been reported to be responsible of their higher catalytic performance (Pan and Bao, 2011; Fu et al., 2013; Xiao et al., 2015). A comparative study of the catalytic behavior of cobalt catalyst supported on graphene and on CNT for the FTS showed that the use of graphene increased the rate by 22%, shifted the product distribution to long-chain hydrocarbons, and exhibited higher stability when compared to CNT, at 220°C, 18 bar, and a H<sub>2</sub>/CO ratio of 2 (Karimi et al., 2015a; Karimi et al., 2015b). These properties were attributed to a better dispersion of cobalt clusters and to an increase in the degree of reduction of Co at relatively lower temperatures in the graphene-supported catalyst. Nevertheless, the TOF values reported in this work for Co-supported on graphene and CNTs (38.6 and 35.1 s<sup>-1</sup>, respectively) were quite far from the range of TOF values (25 × 10<sup>-3</sup>–160 × 10<sup>-3</sup> s<sup>-1</sup>) reported for Co/CNTs under similar reaction conditions (Supplementary Figure S1A). In this sense, the poorly crystallized graphitic (amorphous) structure of ACs and OMCs does not seem to be a favorable characteristic for a catalyst support in FTS (Zaman et al., 2009; Fu et al., 2013).

Nevertheless, the unique (meso-) porous structure of the different carbon supports has been suggested to provide geometric constraints that allow controlling the product distribution through the shape selective role of the catalytic system. Particularly, the special confinement effect of CNTs was reported to restrict cobalt particle sintering during catalyst activation and FTS reaction conditions. As compared in Table 1, CNTs had the maximum pore (tube) diameter and most of the metal particles are usually inside the pores (tubes). Therefore, the reaction intermediates formed inside the pores can contact the metal active site for longer time, promoting the formation of long-chain hydrocarbons. Furthermore, the high length-to-diameter ratio in CNTs and CNFs confers them a high external surface area that together with the absence of microporosity significantly reduces the mass transfer limitations compared to those of the traditional microporous activated carbons (Abbaslou et al., 2010). Contrary to this, the confinement of cobalt catalyst inside hollow carbon spheres resulted in higher selectivity to methane associated to an H<sub>2</sub> enrichment effect inside the hollow carbon structure (Phaahlamohlaka et al., 2017; Phaahlamohlaka et al., 2020). Comparatively, the microporous structure in ACs is claimed to result in a higher selectivity to methane and a higher light hydrocarbon fraction, which was attributed to the high specific surface area of these carbon supports, leading to smaller cobalt particle sizes and diffusion limitations for CO as compared to that of H<sub>2</sub> (resulting in a higher H<sub>2</sub>/CO ratio inside the pores) (Zaman et al., 2009; Fu et al., 2013). Similar results were recently reported for Co supported on oxidized and N-doped graphene nanoflakes with narrow pores (Chernyak et al., 2019). However, the wider pore sizes in OMC-supported catalysts led to improved catalyst mass transfer properties and

higher selectivity to long-chain hydrocarbons compared to those of AC-supported catalysts (**Supplementary Tables S1, S2**).

Regarding the use of Fe-supported catalysts, both Fe/CNTs and Fe-MOFMS catalysts present high and similar FeTY values (**Figure 11B**). It has been observed along the reported literature that the proximity between carbon and supported iron particles can facilitate the formation of iron carbides, thus leading to a higher concentration of the iron carbide active phase on the catalyst surface, giving rise to a high selectivity to C<sub>5+</sub> hydrocarbons (Chen et al., 2008; Santos et al., 2015). The Fe nanoparticle confinement in CNTs seems to be an ideal condition for the successful formation of the active iron carbide species. This fact can explain the high FeTY obtained for these catalytic systems. Furthermore, the restricted iron sintering of the iron carbide nanoparticles confined and/or embedded in the carbon matrix in these carbon structures also confers a high catalyst stability. In this regard, it was suggested (Cheng et al., 2014) that the confinement of iron nanoparticles inside the CNT with unique electronic properties presents a more relevant impact on the preparation of more active, selective, and stable FT catalysts than that of iron dispersion.

In line with these observations, iron and cobalt nanoparticles highly dispersed and embedded in CSs and OMCs have been prepared in a single step *via* the hydrothermal synthesis of a mixture of the carbon and the metal precursors. According to this catalyst preparation procedure, the close contact between iron and the carbon can facilitate the easy formation of the active iron carbide phase during the subsequent carbonization stage and in the FTS reaction conditions, resulting in catalysts with a high FTS activity and stability (Yu et al., 2010; Sun et al., 2012; Teng et al., 2018). Contrary to this, a detrimental effect was observed for the case of Co-based catalysts with Co nanoparticles embedded in the carbon matrix, as that reported for Co/OMCs, due to the fact that the metallic cobalt surface is the active phase for Co-based catalysts in FTS reaction. Thus, when Co particles are surrounded by the carbonaceous matrix, a large part of the cobalt active sites are blocked, being deactivated (Liu et al., 2017).

Concerning the use of metal promoters, several authors observed that metal promotion effect is also dependent on the support structure. Nevertheless, the comparison of metal promotion on different carbon-supported catalysts has not been well investigated, which makes difficult the discussion of the effect of metal promotion on different carbon-supported catalysts on FTS performance. For example, sodium promotion was more pronounced on Fe/CNTs as compared to that on Fe/OMC, due to the presence of iron carbide species stabilized by encapsulation in the carbon matrix of the Fe/CNT catalytic system (Cheng et al., 2015). Therefore, higher selectivity values to both light and long-chain olefins were observed for Na-promoted Fe/CNT catalysts when compared to those of Fe/OMC. Likewise, it was found that the iron reducibility and carburization proceeded much easier for iron species confined inside CNTs and promoted with Bi and Pb, which resulted in an increase in FeTY and in a higher selectivity to light olefins (around 40% at 10 bar and 60% at 1 bar, 350°C and H<sub>2</sub>/CO = 1), as compared to those of the promoted and nonconfined catalysts (Gu et al., 2019). This

behavior was attributed to the closer contact of the promoters with Fe inside the tubes due to the nanoconfinement effect. The use of carbon-based supports derived from lignocellulosic biomass in FTS has been less studied. Moreover, the presence of inorganic species in biomass-derived carbon supports might play an important role in enhancing the activity in FTS. Such studies would help to identify suitable biomass sources and natural and cheap promoters from the extensive and heterogeneous diversity of the biomass materials.

Another important aspect related to FT synthesis, which has not been so widely discussed in the literature, is the high exothermicity of the process in relation to heat removal and reactor temperature control. Highly exothermic reactions, such as those of the FTS, usually present important heat-transfer problems, giving rise to hotspots in chemical reactors that may damage the catalysts. In this line, it has been reported that local overheats in Co-based catalytic bed results in the increase of methane selectivity and in an acceleration of catalyst deactivation (Visconti et al., 2011; Fratalocchi et al., 2018). Conventional pelletized catalysts, which usually involve the use of alumina or silica as catalyst support, present certain limitations in relation to heat removal under FT synthesis reaction conditions (Asalieva et al., 2020). In order to tackle this issue, several approaches such as the use of monolithic (Visconti et al., 2011) or foam (Lacroix et al., 2011) structured catalysts and the operation in microchannel reactors (Holmen et al., 2013) have been explored.

The use of carbon materials has been also reported to be a feasible solution to overcome heat-transfer problems in FT reactors. Chin et al. (2005) reported the preparation of microstructured Co-Re catalysts based on aligned multiwall carbon nanotube arrays supported on FeCrAlY foam. A four times higher catalytic activity was obtained for the carbon-containing microstructured catalyst as compared to the one of an engineered catalyst structure without the carbon nanotube arrays. This difference was attributed to the superior thermal conductivity for the carbon-containing microstructured catalyst, which resulted in a higher mass and heat transfer and in an improved reactor temperature control, being it possible to operate at higher temperatures without methane selectivity runaway. In this context, professor Holmen and collaborators have intensively worked on the use of different monolithic/microstructured reactors using carbon-based catalysts (Zarubova et al., 2011; Holmen et al., 2013). They reported the preparation of Co catalysts supported on hierarchically structured carbon nanofibers (CNFs)/carbon felt composites. These materials showed enhanced heat and mass transfer and provided a relatively uniform temperature profile inside the reactor. Similarly, the addition of exfoliated graphite to pelletized Co-based catalysts resulted in a 30 times higher thermal conductivity for the catalytic bed than that of the catalyst without any additives and gave rise to an enhanced catalytic performance (Asalieva et al., 2020).

In the light of all the aforementioned results, one can conclude that carbon materials exhibit a huge potential not only in terms of reducing metal-support interactions and providing a high metal dispersion and FTS catalyst activity, but also for the enhancement of the heat and mass transfer inside the reactor, allowing for a

better reactor temperature control and a higher catalytic performance.

## CONCLUSIONS, CHALLENGES, AND FUTURE PERSPECTIVES

Fischer-Tropsch synthesis (FTS) is an important industrial process in the transformation of nonpetroleum carbon resources, including natural gas, coal, and lignocellulosic biomass into clean hydrocarbon fuels and valuable chemicals. The FTS catalysts are required to be preferably supported, and carbon-based materials have been recognized as an interesting alternative to conventional metal oxides. In this review, we have described the use of different carbon-based materials as supports for Co, Fe, and in a lesser extent Ru-based FT catalysts (promoted and unpromoted) over the past 2 decades, including activated carbons (ACs), ordered mesoporous carbons (OMCs), carbon nanotubes and nanofibers (CNTs and CNFs), carbon spheres (CSs), diamond, grapheme, and graphite. Some general conclusions can be drawn from these studies: (1) the carbon surface modification (functionalization and doping) with oxygen and nitrogen functional groups, especially in the case of carbon supports prepared at high carbonization temperature, is crucial to produce catalysts with a high dispersion, FTS activity, stability, and enhanced selectivity; (2) the extent of reduction of FT metal-carbon catalysts is generally high due to the low metal-support interactions; (3) the proximity between carbon and supported iron can facilitate the formation of the active iron carbides, thus leading to a higher concentration of active sites on the catalyst surface; (4) the morphology and structure of the carbon are crucial aspects to modify the metal-support interactions, the metal dispersion, the particle size, and hence, their performance in the FTS process. Specifically, metal catalyst confinement inside the pores of CNTs has shown an outstanding behavior as compared to those of catalytic systems presenting metal nanoparticles supported on the outer CNT surface; (5) larger pores in the support, as those in CNTs, OMCs, and mesoporous carbon spheres, resulted in larger metal phase crystallites formed inside and, thus, higher metal reducibility and lower metal dispersion, enhancing, on the other hand, the hydrocarbon diffusion and the formation of long-chain hydrocarbons; (6) an optimum metal promoter loading and a close proximity between the promoter and the FT metal catalyst seem to be essential factors to increase the FT catalyst reducibility and, thus, to improve the FTS activity and selectivity; (7) it has been demonstrated that the carbon support improves the catalyst heat-transfer properties during the highly exothermic FTS reaction and, thus, the catalytic performance.

However, there are also some challenges to be addressed and future perspectives regarding the use of carbon-based materials as FTS catalyst supports from an industrial-scale point of view. One of these issues is the low density and, in some cases, the insufficient mechanical strength of carbon-based materials. Most of FT reactors used in industry are fixed-bed reactors and slurry reactors. When using a fixed-bed reactor, the catalyst requires to have an appropriate size and shape and therefore they need to be pelletized in order to facilitate intraparticle mass transfer and avoid high-pressure drops. In

case of using a slurry reactor, problems derived from the catalyst abrasion and product-catalyst separation are remarkable. Carbon-supported catalysts have been less evaluated on a slurry reactor, and these issues need to be investigated.

One important disadvantage is related to the high costs of the nanostructured carbon materials as compared to conventional oxide supports, typically used in the FTS process. Although the industrial production of CNTs, CNFs, and AC is currently not an issue, the production of metal-doped carbons is currently not available on a large industrial scale. Furthermore, in most of the cases, petroleum-derived carbon sources are used for the preparation of the carbon-based materials. Only in the case of ACs, the use of biomass sources has been explored as raw material. Nevertheless, most of the catalysts studied have been prepared using commercially available AC supports. Much research is still necessary in this direction. In this sense, renewable biomass residues, besides being used for the production of liquid fuels *via* gasification and further conversion of the produced syngas, could be used for the production of the FT catalyst supports, resulting in both a positive environmental and an economic impact. By this way, it would be possible to minimize greenhouse gas emissions and to achieve a significant reduction of fossil fuel dependency. On this context, the simulation of syngas from the gasification of biomass as feedstock to the FTS reactor operating at both low- and high-temperature (LT-FTS and HT-FTS) processes, using carbon-based catalyst supports, has not been explored in detailed. Therefore, process intensification and catalyst engineering are both crucial steps necessary to be investigated and optimized for the successful implementation of the biomass-to-liquid technology and the use of carbon-based catalyst supports for FTS at large scale.

## AUTHOR CONTRIBUTIONS

JR-M and TC conceived and designed the structure of the review. MV-R, MR-C, and JP contributed with the literature analysis, illustrations, and writing the manuscript. All authors contributed to the manuscript revision and approved the submitted version.

## ACKNOWLEDGMENTS

The authors acknowledge the Spanish Ministry of Science, Innovation, and Universities (MICIU) and FEDER (Project RTI2018-097555-B-I00) and Junta de Andalucía (Project UMA18-FEDERJA-110). MJVR acknowledges MICIU for her Juan de la Cierva-Incorporación postdoctoral fellowship (IJC2019-041222-I), and MARC thanks MICIU for his FPU predoctoral fellowship (FPU18/02796).

## SUPPLEMENTARY MATERIAL

The Supplementary Material for this article can be found online at: <https://www.frontiersin.org/articles/10.3389/fmats.2020.617432/full#supplementary-material>.

## REFERENCES

- Aasberg-Petersen, K., Christensen, T. S., Dybkjaer, I., Sehested, J., Østberg, M., Coertzen, R. M., et al. (2004). Chapter 4-Synthesis gas production for FT synthesis. *Stud. Surf. Sci. Catal.* 152, 258–405. doi:10.1016/S0167-2991(04)80461-0
- Abbaslou, R. M. M., Soltan, J., and Dalai, A. K. (2010). Effects of nanotubes pore size on the catalytic performances of iron catalysts supported on carbon nanotubes for Fischer–Tropsch synthesis. *Appl. Catal. Gen.* 379, 129–134. doi:10.1016/j.apcata.2010.03.006
- Abbaslou, R. M. M., Tavassoli, A., Soltan, J., and Dalai, A. K. (2009). Iron catalysts supported on carbon nanotubes for Fischer–Tropsch synthesis: effect of catalytic site position. *Appl. Catal. Gen.* 367, 47–52. doi:10.1016/j.apcata.2009.07.025
- Abrokwhah, R. Y., Rahman, M. M., Deshmane, V. G., and Kuila, D. (2019). Effect of titania support on Fischer–Tropsch synthesis using cobalt, iron, and ruthenium catalysts in silicon-microchannel microreactor. *Molecular Catalysis.* 478, 110566. doi:10.1016/j.mcat.2019.110566
- Ahn, C.-I., Park, Y. M., Cho, J. M., Lee, D. H., Chung, C.-H., Cho, B. G., et al. (2016). Fischer-tropsch synthesis on ordered mesoporous cobalt-based catalysts with compact multichannel fixed-bed reactor application: a review. *Catal. Surv. Asia.* 20, 210–230. doi:10.1007/s10563-016-9219-5
- Almkhelfe, H., Li, X., Thapa, P., Hohn, K. L., and Amama, P. B. (2018). Carbon nanotube-supported catalysts prepared by a modified photo-Fenton process for Fischer–Tropsch synthesis. *J. Catal.* 361, 278–289. doi:10.1016/j.jcat.2018.02.009
- Asalieva, E., Sineva, L., Sinichkina, S., Solomonik, I., Gryaznov, K., Pushina, E., et al. (2020). Exfoliated graphite as a heat-conductive frame for a new pelletized Fischer–Tropsch synthesis catalyst. *Appl. Catal. Gen.* 601, 117639. doi:10.1016/j.apcata.2020.117639
- Bahome, M. C., Jewell, L. L., Hildebrandt, D., Glasser, D., and Coville, N. J. (2005). Fischer–Tropsch synthesis over iron catalysts supported on carbon nanotubes. *Appl. Catal. Gen.* 287, 60–67. doi:10.1016/j.apcata.2005.03.029
- Bezemer, G. L., Bitter, J. H., Kuipers, H. P., Oosterbeek, H., Holewijn, J. E., Xu, X., et al. (2006a). Cobalt particle size effects in the Fischer–Tropsch reaction studied with carbon nanofiber supported catalysts. *J. Am. Chem. Soc.* 128, 3956–3964. doi:10.1021/ja058282w
- Bezemer, G. L., Falke, U., Van Dillen, A. J., and De Jong, K. P. (2005). Cobalt on carbon nanofiber catalysts: auspicious system for study of manganese promotion in Fischer–Tropsch catalysis. *Chem. Commun.* 731–733. doi:10.1039/b414788j
- Bezemer, G. L., Radstake, P. B., Falke, U., Oosterbeek, H., Kuipers, H. P. C. E., Van Dillen, A. J., et al. (2006b). Investigation of promoter effects of manganese oxide on carbon nanofiber-supported cobalt catalysts for Fischer–Tropsch synthesis. *J. Catal.* 237, 152–161. doi:10.1016/j.jcat.2005.10.031
- Chen, L., Song, G., Fu, Y., and Shen, J. (2012). The effects of promoters of K and Zr on the mesoporous carbon supported cobalt catalysts for Fischer–Tropsch synthesis. *J. Colloid Interface Sci.* 368, 456–461. doi:10.1016/j.jcis.2011.11.030
- Chen, Q., Liu, G., Ding, S., Chanmiya Sheikh, M., Long, D., Yoneyama, Y., et al. (2018). Design of ultra-active iron-based Fischer–Tropsch synthesis catalysts over spherical mesoporous carbon with developed porosity. *Chem. Eng. J.* 334, 714–724. doi:10.1016/j.cej.2017.10.093
- Chen, W., Fan, Z., Pan, X., and Bao, X. (2008). Effect of confinement in carbon nanotubes on the activity of Fischer–Tropsch iron catalyst. *J. Am. Chem. Soc.* 130, 9414–9419. doi:10.1021/ja8008192
- Chen, W., Pan, X., and Bao, X. (2007). Tuning of redox properties of iron and iron oxides via encapsulation within carbon nanotubes. *J. Am. Chem. Soc.* 129, 7421–7426. doi:10.1021/ja0713072
- Chen, W., Pan, X., Willinger, M. G., Su, D. S., and Bao, X. (2006). Facile autoreduction of iron oxide/carbon nanotube encapsulates. *J. Am. Chem. Soc.* 128, 3136–3137. doi:10.1021/ja0567211
- Cheng, K., Ordonsky, V. V., Legras, B., Virginie, M., Paul, S., Wang, Y., et al. (2015). Sodium-promoted iron catalysts prepared on different supports for high temperature Fischer–Tropsch synthesis. *Appl. Catal. Gen.* 502, 204–214. doi:10.1016/j.apcata.2015.06.010
- Cheng, K., Ordonsky, V. V., Virginie, M., Legras, B., Chernavskii, P. A., Kazak, V. O., et al. (2014). Support effects in high temperature Fischer–Tropsch synthesis on iron catalysts. *Appl. Catal. Gen.* 488, 66–77. doi:10.1016/j.apcata.2014.09.033
- Cheng, Q., Zhao, N., Lyu, S., Tian, Y., Gao, F., Dong, L., et al. (2019). Tuning interaction between cobalt catalysts and nitrogen dopants in carbon nanospheres to promote Fischer–Tropsch synthesis. *Appl. Catal. B Environ.* 248, 73–83. doi:10.1016/j.apcatb.2019.02.024
- Chernavskii, P. A., Pankina, G. V., Kazantsev, R. V., and Eliseev, O. L. (2018). Potassium as a structural promoter for an iron/activated carbon catalyst: unusual effect of component deposition order on magnetite particle size and catalytic behavior in Fischer–Tropsch synthesis. *ChemCatChem.* 10, 1313–1320. doi:10.1002/cctc.201701818
- Chernyak, S. A., Ivanov, A. S., Maksimov, S. V., Maslakov, K. I., Isaikina, O. Y., Chernavskii, P. A., et al. (2020). Fischer–Tropsch synthesis over carbon-encapsulated cobalt and iron nanoparticles embedded in 3D-framework of carbon nanotubes. *J. Catal.* 389, 270–284. doi:10.1016/j.jcat.2020.06.011
- Chernyak, S. A., Stolbov, D. N., Ivanov, A. S., Klokov, S. V., Egorova, T. B., Maslakov, K. I., et al. (2019). Effect of type and localization of nitrogen in graphene nanoflake support on structure and catalytic performance of Co-based Fischer–Tropsch catalysts. *Catal. Today.* 357, 193–202. doi:10.1016/j.cattod.2019.02.044
- Chernyak, S. A., Suslova, E. V., Ivanov, A. S., Egorov, A. V., Maslakov, K. I., Savilov, S. V., et al. (2016). Co catalysts supported on oxidized CNTs: evolution of structure during preparation, reduction and catalytic test in Fischer–Tropsch synthesis. *Appl. Catal. Gen.* 523, 221–229. doi:10.1016/j.apcata.2016.06.012
- Chew, L. M., Xia, W., Dudder, H., Weide, P., Ruland, H., and Muhler, M. (2016). On the role of the stability of functional groups in multi-walled carbon nanotubes applied as support in iron-based high-temperature Fischer–Tropsch synthesis. *Catal. Today* 270, 85–92. doi:10.1016/j.cattod.2015.09.023
- Chin, Y.-H., Hu, J., Cao, C., Gao, Y., and Wang, Y. (2005). Preparation of a novel structured catalyst based on aligned carbon nanotube arrays for a microchannel Fischer–Tropsch synthesis reactor. *Catal. Today* 110, 47–52. doi:10.1016/j.cattod.2005.09.007
- De Jong, K. P., and Geus, J. W. (2000). Carbon nanofibers: catalytic synthesis and applications. *Catal. Rev.* 42, 481–510. doi:10.1081/CR-100101954
- De Smit, E., and Weckhuysen, B. M. (2008). The renaissance of iron-based Fischer–Tropsch synthesis: on the multifaceted catalyst deactivation behaviour. *Chem. Soc. Rev.* 37, 2758–2781. doi:10.1039/b805427d
- Den Breejen, J. P., Radstake, P. B., Bezemer, G. L., Bitter, J. H., Frøseth, V., Holmen, A., et al. (2009). On the origin of the cobalt particle size effects in Fischer–Tropsch catalysis. *J. Am. Chem. Soc.* 131, 7197–7203. doi:10.1021/ja901006x
- Den Breejen, J. P., Sietsma, J. R. A., Friedrich, H., Bitter, J. H., and De Jong, K. P. (2010). Design of supported cobalt catalysts with maximum activity for the Fischer–Tropsch synthesis. *J. Catal.* 270, 146–152. doi:10.1016/j.jcat.2009.12.015
- Díaz, J. A., Akhavan, H., Romero, A., Garcia-Minguillan, A. M., Romero, R., Giroir-Fendler, A., et al. (2014). Cobalt and iron supported on carbon nanofibers as catalysts for Fischer–Tropsch synthesis. *Fuel Process. Technol.* 128, 417–424. doi:10.1016/j.fuproc.2014.08.005
- Dlamini, M. W., Kumi, D. O., Phaahlamohlaka, T. N., Lyadov, A. S., Billing, D. G., Jewell, L. L., et al. (2015). Carbon spheres prepared by hydrothermal synthesis—a support for bimetallic iron cobalt Fischer–Tropsch catalysts. *ChemCatChem.* 7, 3000–3011. doi:10.1002/cctc.201500334
- Dlamini, M. W., Phaahlamohlaka, T. N., Kumi, D. O., Forbes, R., Jewell, L. L., and Coville, N. J. (2020). Post doped nitrogen-decorated hollow carbon spheres as a support for Co Fischer–Tropsch catalysts. *Catal. Today* 342, 99–110.
- Eschemann, T. O., Lamme, W. S., Manchester, R. L., Parmentier, T. E., Cognigni, A., Rønning, M., et al. (2015). Effect of support surface treatment on the synthesis, structure, and performance of Co/CNT Fischer–Tropsch catalysts. *J. Catal.* 328, 130–138. doi:10.1016/j.jcat.2014.12.010
- Eslava, J. L., Fernández-García, M., Guerrero-Ruiz, A., Iglesias Juez, A., and Rodríguez-Ramos, I. (2018). Effect of different promoter precursors in a model Ru-Cs/graphite system on the catalytic selectivity for Fischer–Tropsch reaction. *App. Surf. Sci.* 328, 130–138. doi:10.1016/j.apsusc.2018.03.207
- Figueiredo, J. L., Pereira, M. F. R., Freitas, M. M. A., and Órfão, J. J. M. (1999). Modification of the surface chemistry of activated carbons. *Carbon* 37, 1379–1389. doi:10.1016/S0008-6223(98)00333-9
- Fratallocchi, L., Visconti, C. G., Groppi, G., Lietti, L., and Tronconi, E. (2018). Intensifying heat transfer in Fischer–Tropsch tubular reactors through the adoption of conductive packed foams. *Chem. Eng. J.* 349, 829–837. doi:10.1016/j.cej.2018.05.108

- Fu, T., Jiang, Y., Lv, J., and Li, Z. (2013). Effect of carbon support on Fischer-Tropsch synthesis activity and product distribution over Co-based catalysts. *Fuel Process. Technol.* 110, 141–149. doi:10.1016/j.fuproc.2012.12.006
- Fu, T., Liu, R., Lv, J., and Li, Z. (2014a). Influence of acid treatment on N-doped multi-walled carbon nanotube supports for Fischer-Tropsch performance on cobalt catalyst. *Fuel Process. Technol.* 122, 49–57. doi:10.1016/j.fuproc.2014.01.016
- Fu, T., Lv, J., and Li, Z. (2014b). Effect of carbon porosity and cobalt particle size on the catalytic performance of carbon supported cobalt Fischer-Tropsch catalysts. *Ind. Eng. Chem. Res.* 53, 1342–1350. doi:10.1021/ie402128y
- Geim, A. K., and Novoselov, K. S. (2007). The rise of graphene. *Nat. Mater* 6, 183–191. doi:10.1038/nmat1849
- Ghogia, A. C., Cayez, S., Machado, B. F., Nzihou, A., Serp, P., Soullantia, K., et al. (2020). Hydrogen spillover in the Fischer-Tropsch synthesis on carbon-supported cobalt catalysts. *ChemCatChem*. 12, 1117–1128. doi:10.1002/cctc.201901934
- Gu, B., He, S., Peron, D. V., Strossi Pedrolo, D. R., Moldovan, S., Ribeiro, M. C., et al. (2019). Synergy of nanoconfinement and promotion in the design of efficient supported iron catalysts for direct olefin synthesis from syngas. *J. Catal.* 376, 1–16. doi:10.1016/j.jcat.2019.06.035
- Gu, B., Ordonsky, V. V., Bahri, M., Ersen, O., Chernavskii, P. A., Filimonov, D., et al. (2018). Effects of the promotion with bismuth and lead on direct synthesis of light olefins from syngas over carbon nanotube supported iron catalysts. *Appl. Catal. B Environ* 234, 153–166. doi:10.1016/j.apcatb.2018.04.025
- Hajjar, Z., Doroudian Rad, M., and Soltanali, S. (2017). Novel Co/graphene oxide and Co/nanoporous graphene catalysts for Fischer-Tropsch reaction. *Res. Chem. Intermed* 43, 1341–1353. doi:10.1007/s11164-016-2701-x
- Hernández Mejía, C., Van Deelen, T. W., and De Jong, K. P. (2018). Activity enhancement of cobalt catalysts by tuning metal-support interactions. *Nat. Commun.* 9, 4459. doi:10.1038/s41467-018-06903-w
- Holmen, A., Venvik, H. J., Myrstad, R., Zhu, J., and Chen, D. (2013). Monolithic, microchannel and carbon nanofibers/carbon felt reactors for syngas conversion by Fischer-Tropsch synthesis. *Catal. Today* 216, 150–157. doi:10.1016/j.cattod.2013.06.006
- Honsho, T.-O., Kitano, T., Miyake, T., and Suzuki, T. (2012). Fischer-Tropsch synthesis over Co-loaded oxidized diamond catalyst. *Fuel* 94, 170–177. doi:10.1016/j.fuel.2011.08.045
- Hu, B., Wang, K., Wu, L., Yu, S. H., Antonietti, M., and Titirici, M. M. (2010). Engineering carbon materials from the hydrothermal carbonization process of biomass. *Adv Mater Weinheim* 22, 813–828. doi:10.1002/adma.200902812
- Ismail, A. S. M., Casavola, M., Liu, B., Gloter, A., Van Deelen, T. W., Versluijs, M., et al. (2019). Atomic-scale investigation of the structural and electronic properties of cobalt-iron bimetallic Fischer-Tropsch catalysts. *ACS Catal.* 9, 7998–8011. doi:10.1021/acscatal.8b04334
- Jiang, F., Wang, S., Zheng, J., Liu, B., Xu, Y., and Liu, X. (2020). Fischer-Tropsch synthesis to lower  $\alpha$ -olefins over cobalt-based catalysts: dependence of the promotional effect of promoter on supports. *Catal. Today*. doi:10.1016/j.cattod.2020.03.051
- Jiang, F., Zhang, M., Liu, B., Xu, Y., and Liu, X. (2017). Insights into the influence of support and potassium or sulfur promoter on iron-based Fischer-Tropsch synthesis: understanding the control of catalytic activity, selectivity to lower olefins, and catalyst deactivation. *Catalysis Science & Technology* 7, 1245–1265. doi:10.1039/C7CY00048K
- Jun, S., Joo, S. H., Ryoo, R., Kruk, M., Jaroniec, M., Liu, Z., et al. (2000). Synthesis of new, nanoporous carbon with hexagonally ordered mesostructure. *J. Am. Chem. Soc.* 122, 10712–10713. doi:10.1021/ja002261e
- Jung, H. J., Walker, P. L., and Vannice, A. (1982). CO hydrogenation over well-dispersed carbon-supported iron catalysts. *J. Catal.* 75, 416–422. doi:10.1016/0021-9517(82)90223-8
- Kang, J., Zhang, S., Zhang, Q., and Wang, Y. (2009). Ruthenium nanoparticles supported on carbon nanotubes as efficient catalysts for selective conversion of synthesis gas to diesel fuel. *Angew Chem. Int. Ed. Engl.* 48, 2565–2568. doi:10.1002/anie.200805715
- Kang, S. W., Kim, K., Chun, D. H., Yang, J.-I., Lee, H.-T., Jung, H., et al. (2017). High-performance Fe5C2@CMK-3 nanocatalyst for selective and high-yield production of gasoline-range hydrocarbons. *J. Catal.* 349, 66–74. doi:10.1016/j.jcat.2017.03.004
- Karimi, A., Nasernejad, B., Rashidi, A. M., Tavasoli, A., and Pourkhalil, M. (2014). Functional group effect on carbon nanotube (CNT)-supported cobalt catalysts in Fischer-Tropsch synthesis activity, selectivity and stability. *Fuel* 117, 1045–1051. doi:10.1016/j.fuel.2013.10.014
- Karimi, S., Tavasoli, A., Mortazavi, Y., and Karimi, A. (2015a). Cobalt supported on Graphene – a promising novel Fischer-Tropsch synthesis catalyst. *Appl. Catal. Gen.* 499, 188–196. doi:10.1016/j.apcata.2015.04.024
- Karimi, S., Tavasoli, A., Mortazavi, Y., and Karimi, A. (2015b). Enhancement of cobalt catalyst stability in Fischer-Tropsch synthesis using graphene nanosheets as catalyst support. *Chem. Eng. Res. Des.* 104, 713–722. doi:10.1016/j.cherd.2015.10.016
- Karmakar, S., Sharma, S. M., Teredesai, P. V., and Sood, A. K. (2004). Pressure-induced phase transitions in iron-filled carbon nanotubes: X-ray diffraction studies. *Phys. Rev. B* 69, 165414.
- Knox, J. H., Kaur, B., and Millward, G. R. (1986). Structure and performance of porous graphitic carbon in liquid chromatography. *J. Chromatogr. A* 352, 3–25. doi:10.1016/S0021-9673(01)83368-9
- Kuang, T., Lyu, S., Liu, S., Zhang, Y., Li, J., Wang, G., et al. (2019). Controlled synthesis of cobalt nanocrystals on the carbon spheres for enhancing Fischer-Tropsch synthesis performance. *J. Energy Chem.* 33, 67–73. doi:10.1016/j.jechem.2018.08.012
- Kundu, S., Xia, W., Busser, W., Becker, M., Schmidt, D. A., Havenith, M., et al. (2010). The formation of nitrogen-containing functional groups on carbon nanotube surfaces: a quantitative XPS and TPD study. *Phys. Chem. Chem. Phys.* 12, 4351–4359. doi:10.1039/b923651a
- Lacroix, M., Dreibine, L., De Tymowski, B., Vigneron, F., Edouard, D., Bégin, D., et al. (2011). Silicon carbide foam composite containing cobalt as a highly selective and re-usable Fischer-Tropsch synthesis catalyst. *Appl. Catal. Gen.* 397, 62–72. doi:10.1016/j.apcata.2011.02.012
- Lappas, A., and Heracleous, E. (2016). “18-Production of biofuels via Fischer-Tropsch synthesis: biomass-to-liquids,” in *Handbook of Biofuels Production*. Editors R. Luque, C.S.K. Lin, K. Wilson, and J. Clark Second Edition (Cambridge, United Kingdom: Woodhead Publishing), 549–593.
- Lehman, J. H., Terrones, M., Mansfield, E., Hurst, K. E., and Meunier, V. (2011). Evaluating the characteristics of multiwall carbon nanotubes. *Carbon* 49, 2581–2602. doi:10.1016/j.carbon.2011.03.028
- Li, X., Nisa, M. U., Chen, Y., and Li, Z. (2019). Co-based catalysts supported on silica and carbon materials: effect of support property on cobalt species and Fischer-Tropsch synthesis performance. *Ind. Eng. Chem. Res.* 58, 3459–3467. doi:10.1021/acs.iecr.8b05451
- Lipson, H., and Stokes, A. R. (1942). A new structure of carbon. *Nature* 149, 328. doi:10.1038/149328a0
- Liu, C.-Y., and Li, E. Y. (2020). C-C coupling reactions promoted by CNT-supported bimetallic center in Fischer-Tropsch synthesis. *Sustainable Energy & Fuels* 4, 2638–2644. doi:10.1039/C9SE01289C
- Liu, J., Wang, Z., Yan, X., and Jian, P. (2017). Metallic cobalt nanoparticles imbedded into ordered mesoporous carbon: a non-precious metal catalyst with excellent hydrogenation performance. *J. Colloid Interface Sci.* 505, 789–795. doi:10.1016/j.jcis.2017.06.081
- Lund, C. R. F., and Dumesic, J. A. (1981). Strong oxide-oxide interactions in silica-supported magnetite catalysts. 1. X-ray diffraction and Mossbauer spectroscopy evidence for interaction. *J. Phys. Chem.* 85, 3175–3180. doi:10.1021/j150621a034
- Luo, Q.-X., Guo, L.-P., Yao, S.-Y., Bao, J., Liu, Z.-T., and Liu, Z.-W. (2019). Cobalt nanoparticles confined in carbon matrix for probing the size dependence in Fischer-Tropsch synthesis. *J. Catal.* 369, 143–156. doi:10.1016/j.jcat.2018.11.002
- Luque, R., De La Osa, A. R., Campelo, J. M., Romero, A. A., Valverde, J. L., and Sanchez, P. (2012). Design and development of catalysts for Biomass-To-Liquid-Fischer-Tropsch (BTL-FT) processes for biofuels production. *Energy Environ. Sci.* 5, 5186–5202. doi:10.1039/c1ee02238e
- Lyu, S., Peng, B., Kuang, T., Rappé, K. G., Zhang, Y., Li, J., et al. (2019). Supported cobalt nanoparticles with a single active phase for Fischer-Tropsch synthesis. *ACS Applied Nano Materials* 2, 2266–2272. doi:10.1021/acsnanm.9b00187
- Ma, G., Xu, Y., Wang, J., Bai, J., Du, Y., Zhang, J., et al. (2020). An Na-modified Fe@C core-shell catalyst for the enhanced production of gasoline-range hydrocarbons via Fischer-Tropsch synthesis. *RSC Adv.* 10, 10723–10730. doi:10.1039/D0RA01036G

- Ma, W.-P., Ding, Y.-J., and Lin, L.-W. (2004). Fischer–Tropsch synthesis over activated-carbon-supported cobalt Catalysts: effect of Co loading and promoters on catalyst performance. *Ind. Eng. Chem. Res.* 43, 2391–2398. doi:10.1021/ie034116q
- Ma, W., Kugler, E. L., and Dadyburjor, D. B. (2007). Potassium effects on activated-carbon-supported iron catalysts for Fischer–Tropsch synthesis. *Energy Fuels* 21, 1832–1842. doi:10.1021/ef060654e
- Ma, W., Kugler, E. L., Wright, J., and Dadyburjor, D. B. (2006). Mo–Fe catalysts supported on activated carbon for synthesis of liquid fuels by the Fischer–Tropsch Process: effect of Mo addition on reducibility, activity, and hydrocarbon selectivity. *Energy Fuels* 20, 2299–2307. doi:10.1021/ef0602372
- Malek Abbaslou, R. M., Soltan, J., and Dalai, A. K. (2011). Iron catalyst supported on carbon nanotubes for Fischer–Tropsch synthesis: effects of Mo promotion. *Fuel* 90, 1139–1144. doi:10.1016/j.fuel.2010.10.044
- Malek Abbaslou, R. M., Tavasoli, A., and Dalai, A. K. (2009). Effect of pre-treatment on physico-chemical properties and stability of carbon nanotubes supported iron Fischer–Tropsch catalysts. *Appl. Catal. Gen.* 355, 33–41. doi:10.1016/j.apcata.2008.11.023
- Mohandas, J. C., Gnanamani, M. K., Jacobs, G., Ma, W., Ji, Y., Khalid, S., et al. (2011). Fischer–Tropsch synthesis: characterization and reaction testing of cobalt carbide. *ACS Catal.* 1, 1581–1588. doi:10.1021/cs200236q
- Moreno-Castilla, C., Ferro-García, M. A., Joly, J. P., Bautista-Toledo, I., Carrasco-Marin, F., and Rivera-Utrilla, J. (1995). Activated carbon surface modifications by nitric acid, hydrogen peroxide, and ammonium peroxydisulfate treatments. *Langmuir* 11, 4386–4392. doi:10.1021/la00011a035
- Moreno-Castilla, C., López-Ramón, M. V., and Carrasco-Marín, F. (2000). Changes in surface chemistry of activated carbons by wet oxidation. *Carbon* 38, 1995–2001. doi:10.1016/S0008-6223(00)00048-8
- Moulefera, I., García-Mateos, F. J., Benyoucef, A., Rosas, J. M., Rodríguez-Mirasol, J. M., and Cordero, T. (2020). Effect of Co-solution of carbon precursor and activating agent on the textural properties of highly porous activated carbon obtained by chemical activation of lignin with H<sub>3</sub>PO<sub>4</sub>. *Front. Mater.* 7, 153–154. doi:10.3389/fmats.2020.00153
- Moussa, S. O., Panchakarla, L. S., Ho, M. Q., and El-Shall, M. S. (2014). Graphene-supported, iron-based nanoparticles for catalytic production of liquid hydrocarbons from synthesis gas: the role of the graphene support in comparison with carbon nanotubes. *ACS Catal.* 4, 535–545. doi:10.1021/cs4010198
- Munirathinam, R., Pham Minh, D., and Nzihou, A. (2018). Effect of the support and its surface modifications in cobalt-based Fischer–Tropsch synthesis. *Ind. Eng. Chem. Res.* 57, 16137–16161. doi:10.1021/acs.iecr.8b03850
- Nakhaei Pour, A., Housaindokht, M. R., and Kamali Shahrī, S. M. (2018). Fischer–Tropsch synthesis over cobalt/CNTs catalysts: functionalized support and catalyst preparation effect on activity and kinetic parameters. *Ind. Eng. Chem. Res.* 57, 13639–13649. doi:10.1021/acs.iecr.8b02485
- Noureddin, M. M. B., Elbasher, N. O., and El-Halwagi, M. M. (2014). Optimization and selection of reforming approaches for syngas generation from natural/shale gas. *Ind. Eng. Chem. Res.* 53, 1841–1855. doi:10.1021/ie402382w
- Oschatz, M., Lamme, W. S., Xie, J., Dugulan, A. I., and De Jong, K. P. (2016a). Ordered mesoporous materials as supports for stable iron catalysts in the Fischer–Tropsch synthesis of lower olefins. *ChemCatChem* 8, 2846–2852. doi:10.1002/cctc.201600492
- Oschatz, M., Van Deelen, T. W., Weber, J. L., Lamme, W. S., Wang, G., Goderis, B., et al. (2016b). Effects of calcination and activation conditions on ordered mesoporous carbon supported iron catalysts for production of lower olefins from synthesis gas. *Catalysis Science & Technology* 6, 8464–8473. doi:10.1039/C6CY01251E
- Otun, K. O., Liu, X., and Hildebrandt, D. (2020). Metal-organic framework (MOF)-derived catalysts for Fischer-Tropsch synthesis: recent progress and future perspectives. *J. Energy Chem.* 51, 230–245. doi:10.1016/j.jechem.2020.03.062
- Palomo, J., Ternero-Hidalgo, J. J., Rosas, J. M., Rodríguez-Mirasol, J., and Cordero, T. (2017). Selective nitrogen functionalization of phosphorus-containing activated carbons. *Fuel Process. Technol.* 156, 438–445. doi:10.1016/j.fuproc.2016.10.006
- Pan, X., and Bao, X. (2011). The effects of confinement inside carbon nanotubes on catalysis. *Acc. Chem. Res.* 44, 553–562. doi:10.1021/ar100160t
- Phaahlamohlaka, T. N., Dlamini, M. W., Kumi, D. O., Forbes, R., Jewell, L. L., and Coville, N. J. (2020). Co inside hollow carbon spheres as a Fischer–Tropsch catalyst: spillover effects from Ru placed inside and outside the HCS. *Appl. Catal. Gen.* 599, 117617. doi:10.1016/j.apcata.2020.117617
- Phaahlamohlaka, T. N., Kumi, D. O., Dlamini, M. W., Forbes, R., Jewell, L. L., Billing, D. G., et al. (2017). Effects of Co and Ru intimacy in Fischer–Tropsch catalysts using hollow carbon sphere supports: assessment of the hydrogen spillover processes. *ACS Catal.* 7, 1568–1578. doi:10.1021/acscatal.6b03102
- Prieto, G., Martínez, A., Concepción, P., and Moreno-Tost, R. (2009). Cobalt particle size effects in Fischer–Tropsch synthesis: structural and *in situ* spectroscopic characterisation on reverse micelle-synthesised Co/ITQ-2 model catalysts. *J. Catal.* 266, 129–144. doi:10.1016/j.jcat.2009.06.001
- Ren, J., Cao, J.-P., Zhao, X.-Y., Yang, F.-L., and Wei, X.-Y. (2019). Recent advances in syngas production from biomass catalytic gasification: a critical review on reactors, catalysts, catalytic mechanisms and mathematical models. *Renew. Sustain. Energy Rev.* 116, 109426. doi:10.1016/j.rser.2019.109426
- Rodríguez-Reinoso, F., and Molina-Sabio, M. (1992). Activated carbons from lignocellulosic materials by chemical and/or physical activation: an overview. *Carbon* 30, 1111–1118. doi:10.1016/0008-6223(92)90143-K
- Rosas, J. M., Bedia, J., Rodríguez-Mirasol, J., and Cordero, T. (2010). On the preparation and characterization of chars and activated carbons from orange skin. *Fuel Process. Technol.* 91, 1345–1354. doi:10.1016/j.fuproc.2010.05.006
- Rosas, J. M., Bedia, J., Rodríguez-Mirasol, J., and Cordero, T. (2008). Preparation of hemp-derived activated carbon monoliths. Adsorption of water vapor. *Ind. Eng. Chem. Res.* 47, 1288–1296. doi:10.1021/ie070924w
- Santos, V. P., Wezendonk, T. A., Jaén, J. J., Dugulan, A. I., Nasalevich, M. A., Islam, H. U., et al. (2015). Metal organic framework-mediated synthesis of highly active and stable Fischer–Tropsch catalysts. *Nat. Commun.* 6, 6451. doi:10.1038/ncomms7451
- Sartipi, S., Makkee, M., Kapteijn, F., and Gascon, J. (2014). Catalysis engineering of bifunctional solids for the one-step synthesis of liquid fuels from syngas: a review. *Catalysis Science & Technology* 4, 893–907. doi:10.1039/C3CY01021J
- Schulte, H. J., Graf, B., Xia, W., and Muhler, M. (2012). Nitrogen- and oxygen-functionalized multiwalled carbon nanotubes used as support in iron-catalyzed, high-temperature Fischer–Tropsch synthesis. *ChemCatChem* 4, 350–355. doi:10.1002/cctc.201100275
- Serp, P., Corrias, M., and Kalck, P. (2003). Carbon nanotubes and nanofibers in catalysis. *Appl. Catal. Gen.* 253, 337–358. doi:10.1016/S0926-860X(03)00549-0
- Serp, P., Feurer, R., Kalck, P., Kihn, Y., Faria, J. L., and Figueiredo, J. L. (2001). A chemical vapour deposition process for the production of carbon nanospheres. *Carbon* 39, 621–626. doi:10.1016/S0008-6223(00)00324-9
- Shariati, J., Haghtalab, A., and Mosayebi, A. (2019). Fischer–Tropsch synthesis using Co and Co–Ru bifunctional nanocatalyst supported on carbon nanotube prepared via chemical reduction method. *J. Energy Chem.* 28, 9–22. doi:10.1016/j.jechem.2017.10.001
- Steynberg, A. P. (2004). “Chapter 1-introduction to Fischer-Tropsch technology,” in *Studies in Surface Science and Catalysis*. Editors A. Steynberg and M. Dry (Amsterdam, Netherlands: Elsevier), 1–63.
- Steynberg, A. P., Espinoza, R. L., Jager, B., and Vosloo, A. C. (1999). High temperature Fischer–Tropsch synthesis in commercial practice. *Appl. Catal. Gen.* 186, 41–54. doi:10.1016/S0926-860X(99)00163-5
- Sun, S., Tsubaki, N., and Fujimoto, K. (2000). The reaction performances and characterization of Fischer–Tropsch synthesis Co/SiO<sub>2</sub> catalysts prepared from mixed cobalt salts. *Appl. Catal. Gen.* 202, 121–131. doi:10.1016/S0926-860X(00)00455-5
- Sun, Z., Sun, B., Qiao, M., Wei, J., Yue, Q., Wang, C., et al. (2012). A general chelate-assisted co-assembly to metallic nanoparticles-incorporated ordered mesoporous carbon catalysts for Fischer–Tropsch synthesis. *J. Am. Chem. Soc.* 134, 17653–17660. doi:10.1021/ja306913x
- Tauster, S. J., Fung, S. C., Baker, R. T., and Horsley, J. A. (1981). Strong interactions in supported-metal catalysts. *Science* 211, 1121–1125. doi:10.1126/science.211.4487.1121
- Tavasoli, A., Trépanier, M., Dalai, A. K., and Abatzoglou, N. (2010). Effects of confinement in carbon nanotubes on the activity, selectivity, and lifetime of Fischer–Tropsch Co/carbon nanotube catalysts. *J. Chem. Eng. Data* 55, 2757–2763. doi:10.1021/je900984c
- Tavasoli, A., Trépanier, M., Malek Abbaslou, R. M., Dalai, A. K., and Abatzoglou, N. (2009). Fischer–Tropsch synthesis on mono- and bimetallic Co and Fe catalysts supported on carbon nanotubes. *Fuel Process. Technol.* 90, 1486–1494. doi:10.1016/j.fuproc.2009.07.007

- Teng, X., Huang, S., Wang, J., Wang, H., Zhao, Q., Yuan, Y., et al. (2018). Fabrication of Fe<sub>2</sub>C embedded in hollow carbon spheres: a high-performance and stable catalyst for Fischer-Tropsch synthesis. *ChemCatChem*. 10, 3883–3891. doi:10.1002/cctc.201800488
- Tian, Z., Wang, C., Si, Z., Ma, L., Chen, L., Liu, Q., et al. (2017). Fischer-Tropsch synthesis to light olefins over iron-based catalysts supported on KMnO<sub>4</sub> modified activated carbon by a facile method. *Appl. Catal. Gen.* 541, 50–59. doi:10.1016/j.apcata.2017.05.001
- Torres Galvis, H. M., Bitter, J. H., Davidian, T., Ruitenbeek, M., Dugulan, A. I., and De Jong, K. P. (2012a). Iron particle size effects for direct production of lower olefins from synthesis gas. *J. Am. Chem. Soc.* 134, 16207–16215. doi:10.1021/ja304958u
- Torres Galvis, H. M., Bitter, J. H., Khare, C. B., Ruitenbeek, M., Dugulan, A. I., and De Jong, K. P. (2012b). Supported iron nanoparticles as catalysts for sustainable production of lower olefins. *Science* 335, 835–838. doi:10.1126/science.1215614
- Trépanier, M., Dalai, A. K., and Abatzoglou, N. (2010). Synthesis of CNT-supported cobalt nanoparticle catalysts using a microemulsion technique: role of nanoparticle size on reducibility, activity and selectivity in Fischer-Tropsch reactions. *Appl. Catal. Gen.* 374, 79–86. doi:10.1016/j.apcata.2009.11.029
- Trépanier, M., Tavasoli, A., Dalai, A. K., and Abatzoglou, N. (2009a). Co, Ru and K loadings effects on the activity and selectivity of carbon nanotubes supported cobalt catalyst in Fischer-Tropsch synthesis. *Appl. Catal. Gen.* 353, 193–202. doi:10.1016/j.apcata.2008.10.061
- Trépanier, M., Tavasoli, A., Dalai, A. K., and Abatzoglou, N. (2009b). Fischer-Tropsch synthesis over carbon nanotubes supported cobalt catalysts in a fixed bed reactor: influence of acid treatment. *Fuel Process. Technol.* 90, 367–374. doi:10.1016/j.fuproc.2008.10.012
- Ugarte, D. (1992). Curling and closure of graphitic networks under electron-beam irradiation. *Nature* 359, 707–797. doi:10.1038/359707a0
- Valero-Romero, M. J., Cabrera-Molina, A., Guerrero-Pérez, M. O., Rodríguez-Mirasol, J., and Cordero, T. (2014). Carbon materials as template for the preparation of mixed oxides with controlled morphology and porous structure. *Catal. Today* 227, 233–241. doi:10.1016/j.cattod.2013.10.093
- Valero-Romero, M. J., García-Mateos, F. J., Rodríguez-Mirasol, J., and Cordero, T. (2017). Role of surface phosphorus complexes on the oxidation of porous carbons. *Fuel Process. Technol.* 157, 116–126. doi:10.1016/j.fuproc.2016.11.014
- Valero-Romero, M. J., Márquez-Franco, E. M., Bedia, J., Rodríguez-Mirasol, J., and Cordero, T. (2014b). Hierarchical porous carbons by liquid phase impregnation of zeolite templates with lignin solution. *Microporous Mesoporous Mater* 196, 68–78. doi:10.1016/j.micromeso.2014.04.055
- Valero-Romero, M. J., Sartipi, S., Sun, X., Rodríguez-Mirasol, J., Cordero, T., Kapteijn, F., et al. (2016). Carbon/H-ZSM-5 composites as supports for bifunctional Fischer-Tropsch synthesis catalysts. *Catalysis Science & Technology* 6, 2633–2646. doi:10.1039/C5CY01942G
- Van Deelen, T. W., Hernández Mejía, C., and De Jong, K. P. (2019). Control of metal-support interactions in heterogeneous catalysts to enhance activity and selectivity. *Nature Catalysis* 2, 955–970. doi:10.1038/s41929-019-0364-x
- Van Deelen, T. W., Yoshida, H., Oord, R., Zečević, J., Weckhuysen, B. M., and De Jong, K. P. (2020). Cobalt nanocrystals on carbon nanotubes in the Fischer-Tropsch synthesis: impact of support oxidation. *Appl. Catal. Gen.* 593, 117441. doi:10.1016/j.apcata.2020.117441
- Visconti, C. G., Tronconi, E., Groppi, G., Lietti, L., Iovane, M., Rossini, S., et al. (2011). Monolithic catalysts with high thermal conductivity for the Fischer-Tropsch synthesis in tubular reactors. *Chem. Eng. J* 171, 1294–1307. doi:10.1016/j.cej.2011.05.014
- Vosoughi, V., Badoga, S., Dalai, A. K., and Abatzoglou, N. (2016). Effect of pretreatment on physicochemical properties and performance of multiwalled carbon nanotube supported cobalt catalyst for Fischer-Tropsch synthesis. *Ind. Eng. Chem. Res.* 55, 6049–6059. doi:10.1021/acs.iecr.5b04381
- Wang, D., Zhou, X., Ji, J., Duan, X., Qian, G., Zhou, X., et al. (2015). Modified carbon nanotubes by KMnO<sub>4</sub> supported iron Fischer-Tropsch catalyst for the direct conversion of syngas to lower olefins. *J. Mater. Chem.* 3, 4560–4567.
- Wang, T., Ding, Y., Lü, Y., Zhu, H., and Lin, L. (2008). Influence of lanthanum on the performance of Zr-Co/activated carbon catalysts in Fischer-Tropsch synthesis. *J. Nat. Gas Chem.* 17, 153–158. doi:10.1016/S1003-9953(08)60043-2
- Wezendonk, T. A., Sun, X., Dugulan, A. I., Van Hoof, A. J. F., Hensen, E. J. M., Kapteijn, F., et al. (2018). Controlled formation of iron carbides and their performance in Fischer-Tropsch synthesis. *J. Catal.* 362, 106–117. doi:10.1016/j.jcat.2018.03.034
- Xiao, J., Pan, X., Guo, S., Ren, P., and Bao, X. (2015). Toward fundamentals of confined catalysis in carbon nanotubes. *J. Am. Chem. Soc.* 137, 477–482. doi:10.1021/ja511498s
- Xie, J., Torres Galvis, H. M., Koeken, A. C., Kirilin, A., Dugulan, A. I., Ruitenbeek, M., et al. (2016). Size and promoter effects on stability of carbon-nanofiber-supported iron-based Fischer-Tropsch catalysts. *ACS Catal.* 6, 4017–4024. doi:10.1021/acscatal.6b00321
- Xie, W., Zhang, Y., Liew, K., and Li, J. (2012). Effect of catalyst confinement and pore size on Fischer-Tropsch synthesis over cobalt supported on carbon nanotubes. *Sci. China Chem.* 55, 1811–1818. doi:10.1007/s11426-012-4727-2
- Xing, C., Yang, G., Wang, D., Zeng, C., Jin, Y., Yang, R., et al. (2013). Controllable encapsulation of cobalt clusters inside carbon nanotubes as effective catalysts for Fischer-Tropsch synthesis. *Catal. Today* 215, 24–28. doi:10.1016/j.cattod.2013.02.018
- Xiong, H., Jewell, L. L., and Coville, N. J. (2015). Shaped carbons as supports for the catalytic conversion of syngas to clean fuels. *ACS Catal.* 5, 2640–2658. doi:10.1021/acscatal.5b00090
- Xiong, H., Motchelaho, M. a. M., Moyo, M., Jewell, L. L., and Coville, N. J. (2011). Correlating the preparation and performance of cobalt catalysts supported on carbon nanotubes and carbon spheres in the Fischer-Tropsch synthesis. *J. Catal.* 278, 26–40. doi:10.1016/j.jcat.2010.11.010
- Xiong, H., Motchelaho, M. A., Moyo, M., Jewell, L. L., and Coville, N. J. (2014a). Fischer-Tropsch synthesis: iron-based catalysts supported on nitrogen-doped carbon nanotubes synthesized by post-doping. *Appl. Catal. Gen.* 482, 377–386. doi:10.1016/j.apcata.2014.06.019
- Xiong, H., Moyo, M., Motchelaho, M. a. M., Jewell, L. L., and Coville, N. J. (2010). Fischer-Tropsch synthesis over model iron catalysts supported on carbon spheres: the effect of iron precursor, support pretreatment, catalyst preparation method and promoters. *Appl. Catal. Gen.* 388, 168–178. doi:10.1016/j.apcata.2010.08.039
- Xiong, H., Moyo, M., Motchelaho, M. A., Tetana, Z. N., Dube, S. M. A., Jewell, L. L., et al. (2014b). Fischer-Tropsch synthesis: iron catalysts supported on N-doped carbon spheres prepared by chemical vapor deposition and hydrothermal approaches. *J. Catal.* 311, 80–87. doi:10.1016/j.jcat.2013.11.007
- Yang, Q.-H., Hou, P.-X., Bai, S., Wang, M.-Z., and Cheng, H.-M. (2001). Adsorption and capillarity of nitrogen in aggregated multi-walled carbon nanotubes. *Chem. Phys. Lett.* 345, 18–24. doi:10.1016/S0009-2614(01)00848-X
- Yang, Y., Chiang, K., and Burke, N. (2011). Porous carbon-supported catalysts for energy and environmental applications: a short review. *Catal. Today* 178, 197–205. doi:10.1016/j.cattod.2011.08.028
- Yang, Y., Jia, L., Hou, B., Li, D., Wang, J., and Sun, Y. (2014). The effect of nitrogen on the autoreduction of cobalt nanoparticles supported on nitrogen-doped ordered mesoporous carbon for the Fischer-Tropsch synthesis. *ChemCatChem*. 6, 319–327. doi:10.1002/cctc.201300897
- Yang, Y., Jia, L., Meng, Y., Hou, B., Li, D., and Sun, Y. (2012). Fischer-tropsch synthesis over ordered mesoporous carbon supported cobalt catalysts: the role of amount of carbon precursor in catalytic performance. *Catal. Lett.* 142, 195–204. doi:10.1007/s10562-011-0747-3
- Yu, G., Sun, B., Pei, Y., Xie, S., Yan, S., Qiao, M., et al. (2010). Fe(x)O(y)@C spheres as an excellent catalyst for Fischer-Tropsch synthesis. *J. Am. Chem. Soc.* 132, 935–937. doi:10.1021/ja906370b
- Zaman, M., Khodadi, A., and Mortazavi, Y. (2009). Fischer-Tropsch synthesis over cobalt dispersed on carbon nanotubes-based supports and activated carbon. *Fuel Process. Technol.* 90, 1214–1219. doi:10.1016/j.fuproc.2009.05.026
- Zarubova, S., Rane, S., Yang, J., Yu, Y., Zhu, Y., Chen, D., et al. (2011). Fischer-Tropsch synthesis on hierarchically structured cobalt nanoparticle/carbon nanofiber/carbon felt composites. *ChemSusChem*. 4, 935–942. doi:10.1002/cssc.201100046
- Zhang, H., Chu, W., Zou, C., Huang, Z., Ye, Z., and Zhu, L. (2011). Promotion effects of platinum and ruthenium on carbon nanotube supported cobalt catalysts for Fischer-Tropsch synthesis. *Catal. Lett.* 141, 438–444. doi:10.1007/s10562-010-0536-4
- Zhang, H., Lancelot, C., Chu, W., Hong, J., Khodakov, A. Y., Chernavskii, P. A., et al. (2009). The nature of cobalt species in carbon nanotubes and their

- catalytic performance in Fischer–Tropsch reaction. *J. Mater. Chem.* 19, 9241–9249. doi:10.1039/B911355J
- Zhang, Y., Ma, L., Tu, J., Wang, T., and Li, X. (2015). One-pot synthesis of promoted porous iron-based microspheres and its Fischer–Tropsch performance. *Appl. Catal. Gen.* 499, 139–145. doi:10.1016/j.apcata.2015.04.017
- Zhao, J. M., Feng, Z., Huggins, F. E., Shah, N., Huffman, G. P., and Wender, I. (1994). Role of molybdenum at the iron oxide surface. *J. Catal.* 148, 194–197. doi:10.1006/jcat.1994.1200
- Zhao, Y., Huang, S., Wei, L., Zhang, Y., Lin, A., Liu, C., et al. (2020). Highly dispersed CoO on graphitic mesoporous carbon as an efficient catalyst for Fischer–Tropsch synthesis. *Ind. Eng. Chem. Res.* 59, 3279–3286. doi:10.1021/acs.iecr.9b06041
- Zhao, Z., Lu, W., Feng, C., Chen, X., Zhu, H., Yang, R., et al. (2019). Increasing the activity and selectivity of Co-based FTS catalysts supported by carbon materials for direct synthesis of clean fuels by the addition of chromium. *J. Catal.* 370, 251–264. doi:10.1016/j.jcat.2018.12.022

**Conflict of Interest:** The authors declare that the research was conducted in the absence of any commercial or financial relationships that could be construed as a potential conflict of interest.

Copyright © 2021 Valero-Romero, Rodríguez-Cano, Palomo, Rodríguez-Mirasol and Cordero. This is an open-access article distributed under the terms of the Creative Commons Attribution License (CC BY). The use, distribution or reproduction in other forums is permitted, provided the original author(s) and the copyright owner(s) are credited and that the original publication in this journal is cited, in accordance with accepted academic practice. No use, distribution or reproduction is permitted which does not comply with these terms.